UNCLASSIFIED

AD NUMBER
AD374761

CLASSIFICATION CHANGES

TO: `unclassified`

FROM: `confidential`

LIMITATION CHANGES

TO:

`Approved for public release, distribution unlimited`

FROM:

`Distribution authorized to U.S. Gov't. agencies and their contractors; Critical Technology; MAR 1966. Other requests shall be referred to Air Force Rocket Propulsion Laboratory, Attn: RPPR-STINFO, Edwards AFB, CA 93523.`

AUTHORITY

`AFRPL ltr, 7 May 1973; AFRPL ltr, 7 May 1973`

THIS PAGE IS UNCLASSIFIED

AFRPL-TR-66-10

374761

CELLULAR COMBUSTION CHAMBER PROGRAM (PROJECT SCORPIO) PHASE III FINAL REPORT

(U) A SIMPLIFIED CLUSTERING TECHNIQUE FOR ROCKET ENGINE MODULES

MR. DAWEEL GEORGE
MR. LESTER E. TEPE
VERNON L. MAHUGH, LT, USAF
MR. HOWARD V. MAIN

TECHNICAL REPORT AFRPL-TR-66-10

MARCH 1966

AIR FORCE ROCKET PROPULSION LABORATORY
RESEARCH AND TECHNOLOGY DIVISION
AIR FORCE SYSTEMS COMMAND
UNITED STATES AIR FORCE
EDWARDS, CALIFORNIA

NOTICES

When U.S. Government drawings, specifications, or other data are
used for any purpose other than a definitely related Government pro-
curement operation, the Government thereby incurs no responsibility
nor any obligation whatsoever, and the fact that the Government may
have formulated, furnished, or in any way supplied the said drawings,
specifications, or other data, is not to be regarded by implication or
otherwise, or in any manner licensing the holder or any other person
or corporation, or conveying any rights or permission to manufacture,
use, or sell any patented invention that may in any way be related
thereto.

CONFIDENTIAL

AFRPL-TR-66-10

CELLULAR COMBUSTION CHAMBER PROGRAM
(PROJECT SCORPIO)
PHASE II FINAL REPORT

(U) A SIMPLIFIED CLUSTERING TECHNIQUE
FOR ROCKET ENGINE MODULES

MR. DAWEEL GEORGE
MR. LESTER E. TEPE
VERNON L. MAHUGH, LT, USAF
MR. HOWARD V. MAIN

TECHNICAL REPORT AFRPL-TR-66-10

MARCH 1966

AIR FORCE ROCKET PROPULSION LABORATORY
RESEARCH AND TECHNOLOGY DIVISION
AIR FORCE SYSTEMS COMMAND
UNITED STATES AIR FORCE
EDWARDS, CALIFORNIA

CONFIDENTIAL

FOREWORD

The results of investigations conducted on a simplified clustering concept for rocket engine modules, single modules utilizing a transpiration-cooled injector face plate and film-cooled thrust chamber, and an advanced-concept gimballing mechanism called the Cam Ring Gimbal are presented in this report. All studies were conducted on site at the Air Force Rocket Propulsion Laboratory under Project 3058, Task 305802, from August 1963 to November 1965.

In the course of the studies, personnel on the engineering staff have changed. Noteworthy contributions to the program have been made by Lieutenants Charles E. Franklin and Kent H. Smith. Gratitude is expressed to the Test Operations Group at Test Stand 1-5 and the Technical Support Division for their contribution to the successful execution of the project.

This technical report has been reviewed and is approved.

ELWOOD M. DOUTHETT
Colonel, USAF
Commander, AF Rocket Propulsion Laboratory

i

UNCLASSIFIED ABSTRACT

Results of the tests and evaluations performed on (a) a simplified clustering technique for rocket engine modules, (b) single modules utilizing simplified large thrust per element injectors and film-cooled thrust chambers, and (c) a unique thrust vectoring mechanism known as the Cam Ring Gimbal are presented. This third and final phase of the Scorpio Project was conducted primarily to investigate the cellular combustor concept to attain high thrust. The concept was evaluated in Task B of this phase. In Task A, 44 single-module tests were conducted on two 25,000-pound thrust, simplified injectors with a 45L* film-cooled thrust chamber. The 2 injector configurations were a single-element concentric pentad and a 17-element coaxial pattern, which were selected for testing with the film-cooled chamber as a result of the performance characteristics displayed when they were tested with an uncooled chamber under Phase I of this program. The effect of film cooling on performance, the heat-transfer characteristics, combustion stability, and smooth start and cutoff transients were the major areas of interest. The 17-element coaxial injector was ultimately selected for use in evaluating the cluster concept due to its more uniform heat-flux distribution, thereby according a more efficient utilization of the film-coolant fuel, and its start and stability characteristics. Eight of the simplified, proven modules from Task A were clustered around a common zero-length, altitude-compensating, plug nozzle to demonstrate a simplified clustering technique for discrete assemblies. Only two propellant valves were used for the entire cluster — one for the oxidizer, and one for the fuel side. The propellants were transported to the injectors through manifolds. Thirteen hot firings were conducted on the cluster configuration. The propellant feed system displayed stable characteristics, and smooth start and cutoff transients were obtained. All eight chambers primed within 80 milliseconds. Hot-firing performance obtained with the plug nozzle correlated very closely with cold-flow data obtained on a model simulating the Scorpio cluster configuration. Under Task C of this phase, the Cam Ring Gimbal was incorporated with the cluster assembly for evaluation under actual hot-firing conditions. The mechanism consisted of four vertically stacked ring wedges, two of which were movable to obtain thrust vectoring. The concept was demonstrated feasible in seven tests, although the gimbal rate achieved was slower than the design rate at full thrust. The high-energy, cryogenic propellant combination of liquid oxygen and liquid hydrogen was used throughout the program.

TABLE OF CONTENTS

Table of Contents (Cont'd)

LIST OF FIGURES

List of Figures (Cont'd)

List of Figures (Cont'd)

LIST OF TABLES

NOMENCLATURE

Symbols		Units
A_t	Chamber Throat Area	in^2
C	Constant	
C_d	Discharge Coefficient	
C_F	Thrust Coefficient	
C*	Characteristic Velocity	ft/sec
D_E	Module Exit Diameter	in
F	Thrust	lbs
g	Gravitational Acceleration	32.2 ft/sec^2
I_s	Specific Impulse	sec
K	Flowmeter Calibration Constant	ft^3/cyc
L*	Characteristic Length, V_c/A_t	in
L	Lower Ring	
M	Mach Number	
M. R.	Mixture Ratio, $\dot{w}_o/\dot{w}_f$	
N	Number of Modules	
PB	Base Pressure - Plug Nozzle	psia
Pc	Chamber Pressure	psia
Pcs	Stagnation Chamber Pressure at the Throat	psia
ΔP	Pressure Differential	psi
R_M	Momentum Ratio, $\dot{w}_o \dot{v}_o/\dot{w}_f \dot{v}_f$	

NOMENCLATURE (Cont'd)

Symbols		Units
TCW	Combustion Temperature at the Chamber Wall	^{o}F
U	Upper Ring	
V	Volume	in^3
v	Velocity	ft/sec
$\dot{w}_\tau$	Propellant Weight Flow Rate	lb/sec

Greek Letters

γ	Ratio of Specific Heats of the Combustion Gases	
δ	Gap Width Between Cluster Modules	in
ϵ	Area Ratio	
η	Efficiency	
θ	Module Tilt Angle	deg
ρ	Density	lb/ft^3
ω	Prandtl-Meyer Turning Angle	deg

Subscripts

a	Actual
Cl	Cluster
c	Chamber, Contraction
cs	Chamber Throat Stagnation
e	Exit
E	Module Nozzle Exit

NOMENCLATURE (Cont'd)

Subscripts

f	Fuel
M	Module
ni	Nozzle Inlet
o	Oxidizer
s	Specific
S. L.	Sea Level
t	Throat, Total
th	Theoretical

SECTION I

INTRODUCTION

(U) The trend in future missile missions is toward launching larger pay-
loads which execute diversified and versatile assignments. A launch
vehicle having a sophisticated, high-thrust, high-performance propulsion
system is required to meet the imposed demands. The classical approach
to attaining high thrust has been to "scale up" or develop very large single
engines such as the F-1 and M-1. Some inherent problems with this
single-engine approach are:

1. Combustion instability, since no really successful injector scal-
ing procedures have yet been established by the rocket industry.

2. The fabrication time and cost, and quality control requirements
for large, complex engine components tend to increase very rapidly with
increase in thrust level.

3. Transportation and testing costs for feasibility demonstration
and development of large liquid rocket engine components are high.

Other approaches to attaining high thrust are to cluster rocket engines,
as is done on the Saturn, or to use strap-on solid boosters, as is done
on the Titan IIIC.

(U) The high-thrust method which was investigated under Project Scorpio
was the cellular combustor concept of clustering proven, simplified,
discrete, thrust chamber modules around a common nozzle. This ap-
proach appeared to have several advantages in that:

1. Each module could be developed and refined to a high degree of
inherent stability and reliability due to its smaller size.

2. Flexibility in thrust level would be afforded by changing the
number of modules.

1

3.   Segmented testing (partial cluster) in the early stages of feasibility demonstration would reduce the cost of testing.

4.   Altitude-compensating nozzles, plug or forced deflection, could be used in combination with clusters of modules.

To demonstrate the feasibility of the simplified clustering technique, eight proven, simplified injectors and film-cooled thrust chambers, each developing 25,000 pounds of thrust, were clustered around a common zero-length plug nozzle. Only two propellant valves were used for the entire cluster; the propellants were transported to each injector through manifolds. Prior to evaluating the simplified clustering concept, a number of single-module test firings were conducted to determine injector performance and the amount of fuel required to film-cool each thrust chamber. Large thrust per element (LTE) injectors with transpiration-cooled faces were utilized in the tests, which provided additional data on the characteristics of LTE injectors over a spectrum of thrust levels: 25,000, 50,000 (Reference 1) and 200,000 (Reference 2) pounds. The simplified clustering concept evolved as a potential economical means of obtaining a high-performing, high-thrust, propulsion system. To further enhance the performance of the concept, an altitude-compensating plug nozzle was incorporated. The practicality of using a cluster-plug nozzle with discrete modules was studied theoretically and with cold-flow models under contract NAS8-11023 (Reference 3) prior to and concurrently with this phase of the Scorpio project. Further, another item which was incorporated into this Phase III effort was the evaluation of the Cam Ring Gimbal (CRG) under actual hot-fire conditions. The CRG is a unique thrust-vectoring mechanism (developed by the Rocketdyne Division of NAA, Inc.) whose configuration readily lends itself to the circular clustering of rocket engine modules.

(U) The investigation of a simplified clustering technique for rocket engine modules was the objective of the final phase, Phase III, of the Cellular Combustion Chamber Program, which had the overall objective of investigating methods to reduce the development time and cost of large

2

liquid rocket engine components. This three-phase exploratory development program was conducted in-house at the Air Force Rocket Propulsion Laboratory and utilized the high-energy cryogenic propellant combination of liquid oxygen and liquid hydrogen. Phase I, which was completed in February 1965, had the objective of evaluating highly simplified, large thrust per element (LTE) injectors at the 50,000-pound thrust level. Results of the Phase I effort are presented in the report AFRPL-TR-65-149 (Reference 1). The Phase II, 200,000-pound thrust, LTE injector evaluations were conducted to determine the maximum practical size for injector elements. Results of the Phase II effort, which was completed in April 1965, are presented in the report AFRPL-TR-65-199 (Reference 2). The description and findings of the Phase III effort are herein presented.

SECTION II

TASK A, SINGLE -MODULE INVESTIGATION

A. GENERAL.

(U) The single-module investigation was conducted to obtain an injector-thrust chamber assembly capable of long run duration and with high combustion performance. The large thrust per element[1] injector concept and thrust chamber film-cooling concept were utilized. The inverted test position, proven feasible for statically testing thrust chamber assemblies during the Phase I and II tests, was used for 40 of the 44 valid, 25,000-pound thrust level tests of this task.

(U) Two injector configurations, the single-element concentric pentad and 17-element coaxial, were tested with the same film-cooled thrust chamber design. The faceplate of each injector was fabricated from porous stainless-steel fibers, Aeromet 347, to provide adequate faceplate transpiration cooling to prevent erosion. The single-element concentric pentad injector configuration R-14A (Figure 1) was chosen for the initial single-module evaluation as a result of the high combustion efficiency achieved with thi type of pattern during the Phase I, 50,000-pound thrust evaluation tests. However, more pronounced thrust-chamber erosion was sustained than was experienced during the Phase I configuration evaluation, which prevented long-duration testing without an excessive amount of film coolant. Modification of the injector element and enlarging the injector film-coolant holes in line with the chamber hot spots improved the

---

[1] An element is defined as one set of oxidizer and fuel tubes. For example, a single-element pentad injector has four oxidizer tubes impinging on a single fuel tube. A coaxial element consists of one oxidizer tube with a fuel annulus.

4

Figure 1. Single-Element Concentric Pentad Injector, R-14A

situation, but did not completely solve the erosion problem. The 17-element coaxial configuration R-14B (Figure 2) was similar to the 32-element coaxial injector evaluated during Phase I. What was considered to be an improved injector design, using the uncooled Phase I data as reference, resulted in low performance. Six injector modifications were required to attain the minimum performance deemed necessary to properly evaluate the cluster concept.

B. TEST COMPONENTS.

(U) 1. Thrust Chamber No. 6.

This thrust chamber (Figure 3) was designed according to the following specifications:

Thrust, F	25,000 pounds
Chamber Pressure, Pcs	800 psia
Mixture Ratio, M. R.	5:1
Contraction Ratio, ϵ_c	2:1
Characteristic Length, L*	45 inches
Film Coolant, $\%\dot{w}_{f_t}$	15

The inside wall of the stainless-steel chamber was plasma-sprayed with a base layer of molybdenum (.005 inch), intermediate layer of tungsten (.005 inch), and outer layer of zirconia (.005 inch), to provide a thermal barrier between the combustion products and chamber wall. Control of the film-coolant flow rates at each of the three coolant rings was obtained by installing an orifice at the inlet to each ring. The chamber was instrumented with pressure taps, temperature probes, and accelerometers to acquire test data and was stressed for 1000 psig at 1200°F with a minimum safety factor of two. The seal between chamber segments was accomplished with a copper gasket located in a serrated groove in one segment and compressed by a serrated tongue of another segment.

6

Figure 2. Seventeen-Element Coaxial Injector, R-11B

Figure 3. Film-Cooled Thrust Chamber No. 6

8

With the specifications given and the assumptions that $C_a^* = 0.96\ C^*_{th}$ and $I_{s_a} = 0.92\ I_{s_{th}}$, shifting equilibrium theoretical data for LO_2/LH_2 was utilized to determine optimum sea level specific impulse, expansion ratio, and characteristic velocity. The equation

$$\dot{w}_t = \frac{F}{\eta\ I_{s_{th_{S.\ L.}}}} \tag{1}$$

was utilized to determine the total propellant flow rate required. The throat area was obtained from

$$A_t = \frac{\eta_{c^*}C^*\dot{w}_t}{P_c g} \tag{2}$$

after which C_F was calculated from

$$F = P_c A_t C_F. \tag{3}$$

The throat, exit, and chamber diameters for a cylindrical chamber were then determined. In these calculations, no radii were assumed at the entrance to the convergent section and at the throat. Knowing the diameters and contraction ratio, and choosing the convergent and divergent half angles, the lengths of the chamber cylinder, convergent section, and nozzle were calculated. The transition for optimum thrust nozzle contour in the convergent-divergent region was accomplished by using the Roa approximation (Reference 4). The thrust chamber was expanded to an area ratio, ϵ, of 5.5/1.

The chamber was fabricated in four segments. The injector end of the chamber, segment number 1, was cooled by fuel flowing from holes drilled at the periphery of the injector. To film-cool the remaining chamber segments 2, 3, and 4, three stations along the chamber wall were provided for fuel injection. Fuel entering the station manifolds was channeled through passageways to three respective rings, each having 90 holes tangent to and directed axially along the inside chamber wall toward the throat. Two orifice metering methods were used to control the film-coolant flow rate to each station. The first method consisted of an orifice

9

plate located between two flanges. This method was later replaced by the simplified dishpan orifice assembly shown in Figure 4. The dishpan orifice was adopted because (1) time and effort to change orifices were reduced, (2) the orifices were reusable, and (3) accuracy of orifice diameter when torqued into the film-coolant manifold was maintained.

(U) 2. Injectors.

a. Injector Design Approach. Information obtained from the Phase I injector evaluations served as preliminary basis for the design of the two 25,000-pound thrust injectors evaluated under this Phase. The two injector designs and their modifications are described below. Table I presents the detailed design data for each injector.

Both injector bodies were fabricated from stainless-steel (AISI 347) material. The porous faceplates were fabricated from 347 stainless-steel fibers (Aeromet 347) to provide for injector face tran- spiration cooling. Twenty percent of the total fuel flow rate was assumed for cooling the injector-chamber assembly--5% was provided at the injector for faceplate cooling and chamber-segment-1 film cooling, and 15% was provided to film-cool thrust chamber segments 2, 3, and 4. The fuel and oxidizer injector tube sizes were then calculated using the remaining fuel and total oxidizer propellant flow rates; therefore, the injector mixture ratio was higher than the overall or total mixture ratio for the injector-chamber assembly. Each injector was stressed for 1200 psig at ambient temperature, utilizing a safety factor of two. A copper gasket provided the seal between the injector flange serrated tongue and the chamber flange serrated groove. Each manifold, fuel and oxidizer, was instrumented with fittings for temperature probes and pressure taps.

b. Single-Element Concentric Pentad, R-14A. Due to the high combustion performance obtained with this injector pattern when tested at the 50,000-pound thrust level (Reference 1), it was chosen for further evaluation in this Phase III task. Figure 1 shows the single-element injector pattern designed to deliver 25,000 pounds of thrust at 800 psia

10

Figure 4. Dishpan Orifice Assembly

Injector Configuration	P_{cs} psia	Thrust lb.	M.R. Overall	R_M*	Exit $A_{o_{inj}}$ in.^{2}	Exit $A_{f_{inj}}$ in^2	ΔP_o psi	ΔP_f psi	Exit $V_{o_{inj}}$ ft/sec	Exit $V_{f_{i}}$ ft/
R - 14A	800	25K	5	4.0	1.453	1.216	80	60	84.3	295
R - 14A, Modified	750	25K	4	3.5	1.453	1.877	80	40	80.8	212
R - 14B	800	25K	5	-	1.123	0.662	150	150	115	475
R - 14C	700	25K	4	-	1.877	0.662	200	170	60	495
R - 14D	700	25K	4	-	1.877	0.662	160	170	60	495
R - 14E	700	25K	4	-	1.877	0.662	100	250	60	495
R - 14F	700	25K	4	-	1.877	0.893	160	190	60	370
R - 14G	700	25K	4	-	1.877	0.893	140	150	60	370
R - 14H	700	25K	4	-	1.877	1.038	140	110	60	315

* The momentum ratio parameter, $R_M = \dfrac{\dot{w}_o v_o}{w_{fct} v_{fct}}$, is applied only t

impinging type injector pattern and is based on the flow throu

fuel center tube (fct).

A_{fat} = Area of fuel annular tubes

$A_{f.c.}$ = Area for film cooling

(U) TABLE I   25,000-POUND THRUST INJECTOR DESIGN DATA

Exit $A_{f_{inj}}$ in^2	ΔP_o psi	ΔP_f psi	Exit $V_{o_{inj}}$ ft/sec	Exit $V_{f_{inj}}$ ft/sec	L/D_o	L/D_f	$\angle$ of Impinge.	$\%\dot{w}t_{fc_{inj}}$	Cd_o	Cd_f	No. of Elements	Remarks
1.216	80	60	84.3	295	7.0	3.0	60°	1.9	.80	.80	1	Single-Elemen (96 holes @
1.877	80	40	80.8	212	6.4	1.9	60°	2.9	.80	.75	1	Single-Elemen (64 holes @
0.662	150	150	115	475	11.1	9.1	-	.83	.80	.80	17	Seventeen-Ele
0.662	200	170	60	495	10.0	9.1	-	-	.57	.80	17	
0.662	160	170	60	495	10.3	9.1	-	-	.65	.80	17	
0.662	100	250	60	495	9.2	9.1	.	-	.72	.56	17	
0.893	160	190	60	370	9.2	7.1	-	-	.59	.69	17	
0.893	140	150	60	370	8.6	7.1	-	-	.41	.63	17	
1.038	140	110	60	315	8.6	6.3	-	-	.41	.64	17	

, $R_M = \dfrac{\dot{w}_o v_o}{w_{fct} v_{fct}}$, is applied only to the

ttern and is based on the flow through the

tubes

ng

2

Cd_o	Cd_f	No. of Elements	Remarks
	.80	1	Single-Element Concentric Pentad, $A_{fct} = .515in^2$, $A_{fat} = .535in^2$, and $A_{f.c.} = .166in^2$ (96 holes @ .047 in. dia.)
	.75	1	Single-Element Concentric Pentad, $A_{fct} = 1.010in^2$, $A_{fat} = .535in^2$, and $A_{f.c.} = .332in^2$ (64 holes @ .047 in.dia. and 32 holes @ .094 in.dia.)
	.80	17	Seventeen-Element Coaxial, see Figure 16 for the various element modifications.
	.80	17	
	.80	17	
	.56	17	
	.69	17	
	.63	17	
	.64	17	

3

chamber pressure. Fuel is injected into the thrust chamber from the center tube and from each annulus shrouding the four 60° impinging oxidizer tubes. The fuel passing through the annuli is used primarily to prevent oxidizer tube erosion. Two modifications were made. The first was to increase the amount of injector film coolant in the area between each oxidizer tube. This is where local hot spots appeared on the thrust chamber wall during the previous tests. The second modification was to the element, and consisted of increasing the fuel center tube diameter from 0.81 to 1.134 inches and recessing the oxidizer tubes..125 inch from the exit plane of the fuel annuli.

        c.   Seventeen-Element Coaxial, R-14B. This injector pattern, Figure 2, is similar to the 32-element coaxial injector tested during Phase I at the 50, 000-pound thrust level. The thrust per element is 1470 pounds at a stagnation chamber pressure of 800 psia and overall mixture ratio of 5:1, oxidizer to fuel. An annulus of fuel surrounds each oxidizer tube. Mixing takes place by shearing action between propellants as a result of the difference in propellant velocities, and by interaction between elements. Each element is angled such that the centerline of the elements impinge at the center of the thrust chamber throat. This was done to eliminate possible thrust chamber streak erosion. The oxidizer tubes were recessed .125 inch from the injector face to provide more efficient propellant mixing. The injector film-coolant holes drilled at the preiphery of the injector faceplate were subsequently eliminated due to the cool wall temperatures recorded in the first chamber segment. A substantial amount of injector modification and testing was pursued with this injector pattern which ultimately was used during the cluster concept demonstration. Single-element cold-flow models using water and gaseous nitrogen to simulate liquid oxygen and liquid hydrogen, respectively, were fabricated to investigate propellant mixing characteristics prior to design modifications and hot firing of the injectors. Figures 5 and 6 show the increase in propellant mixing of the "F" mod element when compared to the original element design flow tested at the same conditions. Table I,

Figure 5. Coaxial Single-Element Model, GN_2/H_2O Test, Mod. F. Manifold

Pressure: $H_2O = 80$ psi and $GN_2 = 150$ psi

16

Figure 6. Coaxial Single-Element Model, GN_2/H_2O Test, Original Design. Manifold Pressure: H_2O = 80 psi and GN_2 = 150 psi

CONFIDENTIAL

Injector Design Data, presents in detail the design changes for each
injector modification. The configuration adopted to demonstrate the
cluster concept consisted of a .489-inch-diameter fuel annulus and a
.375-inch-diameter oxidizer tube recessed .125 inch from the injector
face. The annulus gap was .037 inch.

C. TEST PROGRAM.

(U) 1. General. The evaluation portion of this task consisted of 44 test
firings utilizing the thrust chamber design and two injector configurations
previously described. Both test positions, vertical and inverted,
(a description of the test facility can be found in Reference 1) were
utilized to conduct the evaluation tests. No distinction was made with
regard to the test position in which the injectors were tested. The
testing was conducted over a range of chamber pressures and mixture
ratios to evaluate injector performance and determine the minimum
amount of fuel required to film-cool the thrust chamber. Injector
modifications were made to improve performance, but the designs were
not optimized. An attempt to minimize performance degradation due to
film-cooling the thrust chamber was pursued. A fuel lead on start, and
lag on cutoff, were employed to reduce the possibility of hot-spot erosion
of the thrust chamber during the start and cutoff transients. Steady-state
duration ranged from 1.75 to 4.2 seconds for the single-element concentric
pentad, and from 1.5 to 11.0 seconds for the 17-element coaxial injector.
Instrumentation measurements were taken and performance calculated as
described in paragraph 3. Table II lists the valid test data from the hot
firings conducted. The test results from the injector evaluations and
thrust chamber film-cooling investigations are herein presented.

2. Test Results.

(C) Single-Element Pentad Injector, R-14A. This injector
pattern was tested with the 45L* film-cooled thrust chamber. The com-
bustion efficiency and specific impulse performance obtained with the

CONFIDENTIAL

18

Test. No.	v_o ft/sec	$\triangle P_o$ psi	ρ_o^{man} lb/ft^3	$\dot{w}_o$ lb/sec	v_f ft/sec	$\triangle P_f$ psi	ρ_f^{man} lb/ft^3	$\dot{w}_f$ lb/sec	$\%\dot{w}_t$ fc	R M
R - 14A										
69	69.4	170	66.4	46.2	394	120	3.90	15.6	7.13	1.12
71	76.8	178	67.6	52.4	347	114	4.34	16.4	7.89	1.61
72	-	141	-	51.4	-	-	-	17.2	8.66	-
76	83.9	112	68.3	57.1	325	58.1	4.16	15.1	7.70	2.30
119	77.5	60.7	62.7	49.0	285	63.5	4.46	13.7	8.86	2.30
120	84.9	69.9	61.5	52.7	-	58.7	-	11.7	7.78	-
186	83.9	101	63.7	53.9	228	57.6	4.10	14.2	6.15	2.60
187	77.0	70.0	66.3	51.5	251	66.3	4.10	15.7	6.95	1 87
R -14B										
123	-	99.4	-	50.9	750	189	3.06	14.6	6.16	-
124	96.4	96.4	66.9	50.3	555	193	4.40	15.9	7.18	-
125	103.2	114	68.1	54.8	462	137	4.55	13.9	6.15	-
126	118.0	88.4	67.4	62.0	507	145	4.05	13.2	4.98	-
127	132.3	122	63.2	65.2	520	215	4.26	13.7	4.45	-
128	118.8	101	69.4	64.3	547	165	4.22	13.6	3.83	-
129	130.1	139	67.6	68.6	472	132	4.31	12.3	3.39	-
130	120.6	122	69.3	65.2	437	149	4.65	12.4	3.94	-

(C) TABLE II 25,000-POUND THRUST SINGLE-MODULE TEST RESULTS

$\rho_{f\,man}$ lb/ft³	$\dot{w}_f$ lb/sec	$\%\dot{w}_t$ fc	R M	M.R. overall	P_{cs} psia	F 10³lb	A_{t2} in²	C^*_a ft/sec	C^*_{th} ft/sec	$\%C^*_{th}$	Is_a sec	Is_{th} sec	$\%Is_{th}$
3.90	15.6	7.13	1.12	2.96	610	17.7	20.5	6520	8003	81.5	286	372	76.9
4.34	16.4	7.89	1.61	3.20	695	21.5	20.5	6670	8007	83.3	313	377	83.0
-	17.2	8.66	-	2.99	651	—	20.5	6260	8004	78.2	—	—	—
4.16	15.1	7.70	2.30	3.78	738	23.7	20.5	6760	7986	84.6	328	380	86.3
4.46	13.7	8.86	2.30	3.58	665	20.0	20.5	7020	7997	87.8	319	377	84.6
-	11.7	7.78	-	4.50	669	20.9	20.5	6860	7897	86.9	325	376	86.4
4.10	14.2	6.15	2.60	3.80	709	23.3	20.6	6900	7985	86.4	342	380	90.0
4.10	15.7	6.95	1.87	3.28	730	23.2	20.5	7170	8007	89.6	345	381	90.6
3.06	14.6	6.16	-	3.48	621	20.8	20.4	6250	8002	78.1	318	375	84.8
4.40	15.9	7.18	-	3.16	656	21.3	20.4	6490	8007	81.1	322	375	85.9
4.55	13.9	6.15	-	3.94	641	20.6	20.4	6120	7975	76.7	300	376	79.8
4.05	13.2	4.98	-	4.70	688	21.9	20.4	6000	7865	76.3	291	376	77.4
4.26	13.7	4.45	-	4.76	718	23.1	20.4	5970	7856	76.0	293	377	77.7
4.22	13.6	3.83	-	4.73	715	22.9	20.4	6010	7860	76.5	294	377	78.0
4.31	12.3	3.39	-	5.58	698	22.4	20.4	5650	7675	73.6	277	371	74.7
4.65	12.4	3.94	-	5.26	710	22.8	20.4	6000	7745	77.5	294	374	78.6

ST RESULTS

C*_th	Is_a sec	Is_{th} sec	%Is_{th}	%C_f	E^*_{in}	Steady-State Duration sec	Remarks
.5	286	372	76.9	94.4	45	5.0	No injector erosion, severe chamber erosion
.3	313	377	83.0	99.6	45	4.5	No injector erosion, severe chamber erosion
.2	–	–	–	–	45	3.8	No injector erosion, severe chamber erosion
.6	328	380	86.3	102.0	45	5.0	No injector erosion, severe chamber erosion
7.8	319	377	84.6	96.4	45	1.75	No injector erosion, slight chamber erosion
5.9	325	376	86.4	99.4	45	1.75	No injector erosion, chamber erosion
5.4	342	380	90.9	104.2	45	2.1	No injector erosion, slight chamber erosion
.6	345	381	90.6	101.1	45	4.2	No injector erosion, slight chamber erosion
.1	318	375	84.8	108.6	45	1.5	No injector or chamber erosion
.1	322	375	85.9	105.9	45	6.0	No injector or chamber erosion
5.7	300	376	79.8	104.0	45	6.0	No injector or chamber erosion
5.3	291	376	77.4	101.4	45	6.0	No injector or chamber erosion
.0	293	377	77.7	102.2	45	6.0	No injector or chamber erosion
5.5	294	377	78.0	101.9	45	6.0	No injector or chamber erosion
.6	277	371	74.7	101.5	45	6.0	No injector or chamber erosion
7.5	294	374	78.6	101.4	45	11.0	No injector or chamber erosion

Test No.	v_o ft/sec	ΔP_o psi	ρ_o man lb/ft^3	$\dot{w}_o$ lb/sec	v_f ft/sec	ΔP_f psi	ρ_f man lb/ft^3	$\dot{w}_f$ lb/sec	$\%\dot{w}_t$ fc	R M
		R - 14B con't								
143	123.8	166	65.9	63.6	461	237	4.51	12.9	3.93	-
144	123.7	159	65.6	63.3	587	208	4.08	14.8	4.37	-
150	97.6	123	66.5	50.6	712	403	4.24	17.2	4.66	-
151	99.6	104	67.2	52.2	462	325	4.15	15.7	4.49	-
152	109.4	122	68.1	58.1	629	298	3.83	13.9	3.15	-
		R - 14C								
155	-	190	-	51.3	517	365	3.90	12.3	4.76	-
156	57.2	201	67.9	50.6	485	372	4.22	12.4	3.58	-
		R - 14D								
157	-	176	-	56.5	513	353	3.92	11.8	3.72	-
158	73.7	220	65.8	63.2	468	375	4.10	11.4	3.43	-
159	64.9	153	65.7	55.6	536	372	3.81	11.5	3.14	-
		R - 14E								
170	60.8	160	66.7	52.9	592	342	4.05	13.1	3.13	-
171	59.7	147	66.6	51.8	545	361	4.29	13.0	3.45	-
		R - 14F								
172	57.7	169	66.4	49.9	568	281	4.00	16.0	2.89	-

ρ_f man lb/ft³	$\dot{w}_f$ lb/sec	$\%\dot{w}_t$ fc	R M	M.R. overall	P_c psia	F 10³lb	A_t2 in²	C^*_a ft/sec	C^*_{th} ft/sec	$\%C^*_{th}$	Is_a sec	Is_{th} sec	$\%Is_{th}$
4.51	12.9	3.93	-	4.93	733	23.5	20.4	6280	7823	80.3	307	378	81.2
4.08	16.8	4.37	-	4.28	781	25.2	20.4	6550	7938	82.5	323	383	84.3
4.24	17.2	4.86	-	2.94	732	22.8	20.4	7140	8003	89.2	336	378	88.9
4.15	15.7	4.49	-	3.32	714	23.0	20.6	6960	8006	86.9	339	378	89.7
3.83	13.9	3.15	-	4.18	724	23.2	20.6	6650	7953	83.6	322	379	85.0
3.90	12.3	4.76	-	4.17	668	20.4	20.6	6940	7950	87.3	321	377	85.1
4.22	12.4	3.58	-	4.08	660	20.2	20.6	6930	7959	87.1	321	377	85.1
3.92	11.8	3.72	-	4.79	703	22.1	20.6	6810	7850	86.8	324	378	85.7
4.10	11.4	3.43	-	5.54	743	23.7	20.6	6590	7690	85.7	318	374	85.0
3.81	11.5	3.14	-	4.83	699	21.9	20.6	6880	7844	87.7	326	377	86.5
4.05	13.1	3.13	-	4.04	687	22.1	20.6	6900	7964	86.6	335	380	88.2
4.29	13.0	3.45	-	3.98	676	21.8	20.6	6910	7970	86.7	336	379	88.7
4.00	16.0	2.89	-	3.12	704	22.9	20.6	7080	8007	88.4	347	379	91.6

Is_a sec	Is_{th} sec	$\%Is_{th}$	$\%C_f$	L^* in	Steady-State Duration Sec	REMARKS
307	378	81.2	101.1	45	4.0	No injector or chamber erosion, half injector film-coolant holes plugged
323	383	84.3	102.2	45	4.0	No injector or chamber erosion, half injector film-coolant holes plugged
336	378	88.9	99.7	45	3.0	No injector or chamber erosion, all injector film-coolant holes plugged
339	378	89.7	103.2	45	3.0	No injector or chamber erosion, all injector film-coolant holes plugged
322	379	85.0	101.7	45	3.0	No injector or chamber erosion, all injector film-coolant holes plugged
321	377	85.1	97.5	45	3.0	No injector or chamber erosion, injector film-coolant holes plugged
321	377	85.1	97.7	45	3.0	No injector or chamber erosion, injector film-coolant holes plugged
324	378	85.7	98.7	45	2.5	No injector or chamber erosion, injector film-coolant holes plugged
318	374	85.0	99.2	45	2.5	No injector or chamber erosion, injector film-coolant holes plugged
326	377	86.5	98.6	45	2.5	No injector or chamber erosion, injector film-coolant holes plugged
335	380	88.2	101.8	45	3.8	No injector or chamber erosion, injector film-coolant holes plugged
336	379	88.7	102.3	45	8.3	No injector or chamber erosion, injector film-coolant holes plugged
347	379	91.6	103.6	45	4.3	No injector or chamber erosion, injector film-coolant holes plugged

Test No.	v_o ft/sec	ΔP_o psi	ρ_o man lb/ft³	$\dot{w}_o$ lb/sec	v_f ft/sec	ΔP_f psi	ρ_f man lb/ft³	$\dot{w}_f$ lb/sec	$\%\dot{w}_t$ fc	R M ov
			R - 14F con't							
173	67.5	195	67.1	59.0	379	200	3.91	10.8	2.29	-
174	63.1	181	68.3	56.2	425	228	4.26	13.0	2.56	-
			R - 14G							
175	59.3	175	66.3	51.2	530	258	3.74	13.7	2.16	-
176	-	187	-	57.8	-	217	-	11.6	1.90	-
177	69.4	164	59.1	53.5	479	225	3.84	12.7	2.06	-
178	63.5	178	66.3	54.9	474	247	4.00	12.9	1.67	-
179	70.2	185	65.7	60.1	418	217	3.92	11.2	1.46	-
188	-	156	-	49.9	505	240	3.96	13.5	1.71	-
189	-	162	-	51.7	489	240	4.10	13.8	2.08	-
183	60.6	161	65.6	51.8	603	249	3.59	14.6	1.76	-
184	63.3	157	65.4	54.0	563	249	3.49	13.3	1.65	-
185	56.3	141	67.1	49.2	568	247	3.71	14.2	1.79	-
			R - 14H							
180	58.7	173	68.3	52.3	434	218	3.82	13.0	1.61	-
181	62.7	167	66.4	54.3	422	205	3.94	13.3	1.95	-
182	67.2	172	66.6	58.3	383	198	4.10	12.6	1.81	-

$\rho_{f,man}$ lb/ft³	$\dot{w}_f$ lb/sec	$\%\dot{w}_{t,fc}$	R M	M.R. overall	P_{cs} psia	F 10³lb	A_{t2} in²	C^*_a ft/sec	C^*_{th} ft/sec	$\%C^*_{th}$	Is_a sec	Is_{th} sec	$\%Is_t$
3.91	10.8	2.29	-	5.46	690	22.1	20.6	6550	7702	85.0	317	373	85.0
4.26	13.0	2.56	-	4.32	707	22.7	20.6	6770	7928	85.4	328	380	86.3
3.74	13.7	2.16	-	3.74	697	22.8	20.6	7120	7990	89.1	351	380	92.4
-	11.6	1.90	-	4.98	717	23.2	20.6	6850	7817	87.6	334	377	88.6
3.84	12.7	2.06	-	4.21	699	22.4	20.6	7000	7946	88.1	338	380	88.9
4.00	12.9	1.67	-	4.26	718	23.2	20.6	7020	7942	88.4	342	379	90.2
3.92	11.2	1.46	-	5.37	722	23.5	20.6	6720	7726	87.0	330	373	88.5
3.96	13.5	1.71	-	3.70	682	21.8	20.5	7100	7993	88.8	344	379	90.8
4.10	13.8	2.08	-	3.75	717	22.9	20.5	7230	7990	90.5	350	381	91.9
3.59	14.6	1.76	-	3.55	708	22.9	20.6	7060	7999	88.3	345	380	90.8
3.49	13.3	1.65	-	4.06	705	22.8	20.6	6930	7964	87.0	339	380	89.2
3.71	14.2	1.79	-	3.46	671	21.5	20.6	7010	8002	87.6	339	379	89.4
3.82	13.0	1.61	-	4.02	685	22.0	20.6	6940	7961	87.2	337	379	88.9
3.94	13.3	1.95	-	4.08	710	22.8	20.6	6960	7960	87.4	337	380	88.7
4.10	12.6	1.81	-	4.63	729	23.4	20.6	6800	7887	86.2	330	380	86.8

th	Is_a sec	Is_{th} sec	%Is_{th}	%C_f	L* in	Steady-State Duration sec	Remarks
0	317	373	85.0	100	45	4.2	No injector or chamber erosion
4	328	380	86.3	101.05	45	4.3	No injector or chamber erosion
1	351	380	92.4	103.7	45	4.2	No injector or chamber erosion
6	334	377	88.6	101.1	45	4.2	No injector or chamber erosion
1	338	380	88.9	100.9	45	4.2	No injector or chamber erosion
4	342	379	90.2	192.0	45	4.3	No injector erosion, slight chamber erosion
0	330	373	88.5	101.7	45	4.3	No injector or chamber erosion
8	344	379	90.8	102.3	45	2.4	No injector or chamber erosion
5	350	381	91.9	101.5	45	3.9	No injector or chamber erosion
3	345	380	90.8	102.8	45	4.2	No injector or chamber erosion
0	339	380	89.2	102.5	45	4.2	No injector erosion, slight chamber erosion
6	339	379	89.4	102.1	45	4.2	No injector or chamber erosion
2	337	379	88.9	101.9	45	4.2	No injector or chamber erosion
4	337	380	88.7	101.5	45	4.2	No injector or chamber erosion
2	330	380	86.8	100.7	45	4.2	No injector or chamber erosion

3

CONFIDENTIAL.

original and modified designs are shown in Figures 7 and 8, respectively.
In the eight hot firings conducted with this pattern, overall mixture ratio
was varied from 2.96:1 to 4.5:1, and chamber pressure ranged from 610
to 738 psia. Although no erosion occurred on the injector faceplate or
tubes, significant erosion occurred in the first segment of the thrust
chamber, in local areas 90° apart, where the injector spray fans impinged
on the chamber wall. These hot spots also appeared on the second and
third segments, directly in line with the erosion of the first segment, just
prior to fuel injection from the next coolant ring (see Figures 9 and 10).
In the third and fourth test firings (HF 72 and 76) the chamber film coolant
was redistributed in an attempt to eliminate erosion without further de-
grading performance; no substantial improvement resulted. For hot
firings 119 and 120, the area of the injector periphery film-cooling holes
was doubled, from .166 to .332 square inches, by increasing the hole
diameter over a 30° arc in the four areas between the tubes where hot
spots occurred on the thrust chamber wall. Also, the orifices in the
thrust chamber film-coolant manifolds were changed to redistribute the
fuel where, from observations, more was needed. Post-firing observa-
tions revealed that a slight improvement in cooling effectiveness resulted;
however, further film-coolant perturbations were required. Modifications
were made to the injector element for the final two firings. These consisted
of increasing the fuel center tube area from .515 to 1.010 square inches,
and recessing the oxidizer tubes .125 inch from the exit plane of the fuel
annuli. The thrust chamber film-coolant metering orifices were also
increased. The net effect was that only slight chamber erosion occurred
in a 4.2-second steady-state run (HF 187).

(C) In the process of varying the amount and distribution of
chamber film coolant and modifying the injector, combustion efficiency
and specific impulse performance were increased. The high thrust
coefficient efficiency, $\%C_F$, in some cases greater than 100% (which is
irregular), is attributed to some of the film-coolant fuel completing its
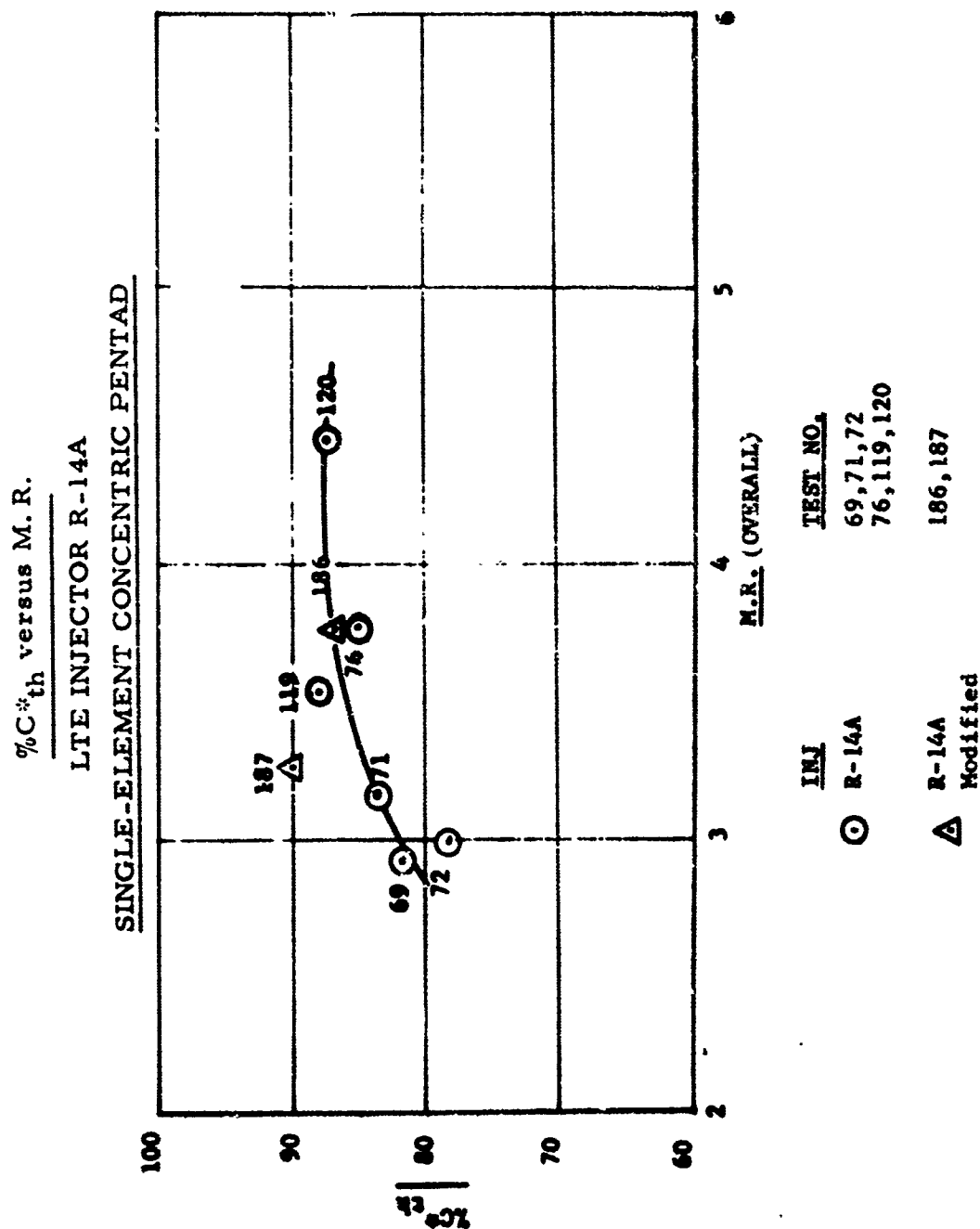combustion in the nozzle (afterburning). Start and cutoff transients

Figure 7. Percent C*th versus Mixture Ratio, Single-Element Concentric Pentad Injecto:

Figure 6. Percent Isth versus Mixture Ratio,
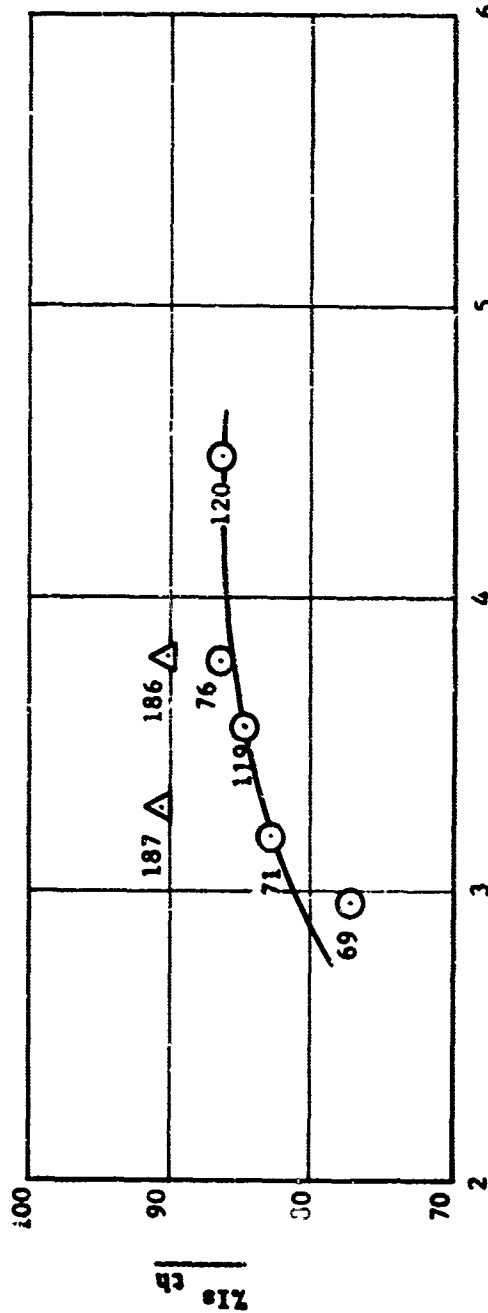Single-Element Concentric Pentad Injector

Figure 9. Thrust Chamber Erosion, Segment 1

Figure 10. Thrust Chamber Erosion, Segments 2 and 3

(This page is Unclassified)

were smooth and maximum steady-state chamber pressure oscillations of
±6.3% were exhibited by the original injector design.

   (C) Seventeen-Element Coaxial Injector, R-14B. The 45L*
film-cooled thrust chamber was also used in the evaluation of this injector
pattern. The combustion efficiency and specific impulse performance which
were obtained are shown in Figures 11 and 12. In the first series of tests,
123 through 130, the performance was low but a trend was observed. As
the overall mixture ratio[2] was increased, performance decreased, although
the amount of fuel used for film-cooling purposes was being decreased. It
also appeared that the film-coolant fuel was not being completely combusted
in the thrust chamber since specific impulse performance was greater than
combustion efficiency, thereby indicating that afterburning was taking place
in the nozzle. Observation of the data obtained from high-response, high-
temperature probes[3] revealed that more than sufficient coolant was being
provided to prevent erosion of the thrust chamber. A typical temperature
profile for this test series is shown in Figure 13. In order to minimize
performance degradation due to film cooling, and avoid thrust chamber
erosion, a desired maximum wall temperature of 1500°F was established
for each chamber segment. Five subsequent tests were then conducted
wherein the quantity and distribution of the film-coolant fuel were varied
to achieve the desired goals. In two progressive steps, film coolant from
the injector was eliminated since the wall temperature in the first chamber
segment was excessively cool. Chamber wall temperatures were
substantially increased and an increase in performance was also obtained.
Figures 14 and 15 give a general indication of the effect film coolant has
on performance for a given mixture ratio. As a result of eliminating the
injector film-coolant holes and reducing the size of the thrust chamber
coolant orifices, injector pressure drop was increased above the tolerable
limit which could be used in the cluster configuration due to test facility

---

[2] The injector end mixture ratio is higher than the overall mixture ratio
     and the difference is directly proportional to the amount of film cooling.

[3] Chamber wall temperatures were measured with Nanmac Type G Chromel
     Alumel probes.

CONFIDENTIAL

Figure 11. Percent C*$_{th}$ versus Mixture Ratio
17-Element Coaxial Injector, R-14B

Figure 12. Percent I$_{sth}$ versus Mixture Ratio,
17-Element Coaxial Injector, R-14B

Figure 13. Thrust Chamber Temperature Profile

33

Figure 14. Percent C^*_{th} versus Film-Coolant Flow Rate

Hot Firing No.	123	124	125	126	127	128	129	130	143	144	150	151	152
M.R. (Overall)	3.48	3.16	3.01	1.72	1.75	1.73	5.58	5.06	1.03	1.28	2.04	3.32	1.18

Figure 15. Percent I_{sth} versus Film-Coolant Flow Rate

Hot Firing No.	123	124	125	126	127	128	129	130	143	144	150	151	152
M.R. (Overall)	3.48	3.16	3.94	4.70	4.76	4.73	5.58	5.26	5.03	4.28	2.24	3.32	4.18

feed system pressure limitations. A step-by-step injector modification
was initiated to alleviate the pressure-drop problem and at the same time
increase performance. With this particular injector pattern, flaring of
the oxidizer and fuel streams takes place in the pre-mix cups, causing
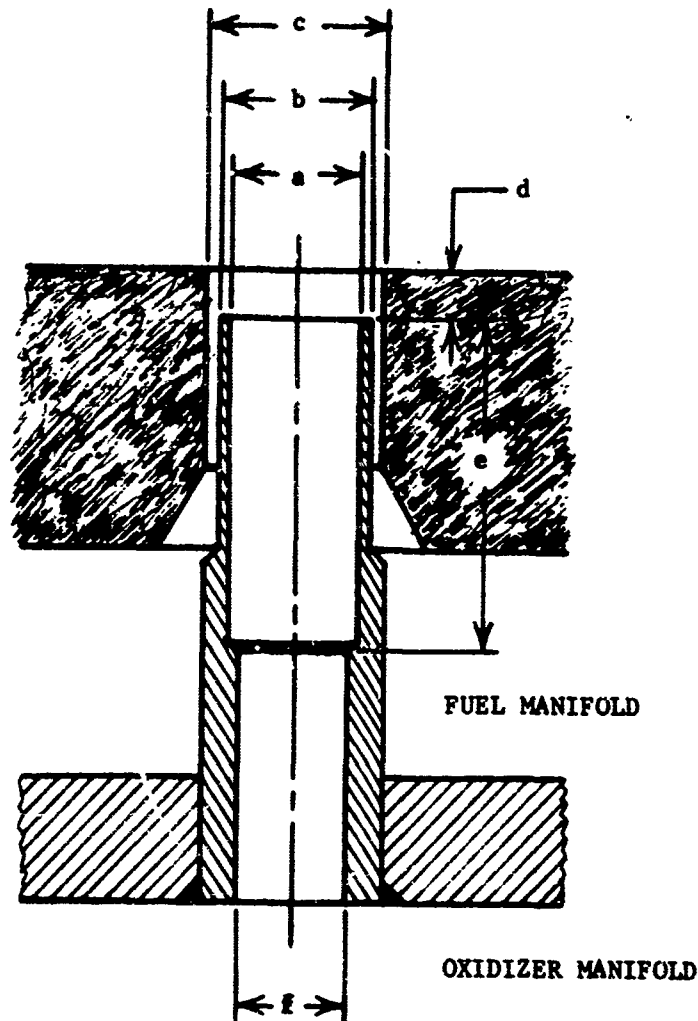hydraulic orificing which results in increased back pressure and reduces
the propellant flow rate. Figure 16 shows the sequential element modifica-
tion that was undertaken. The increase in performance obtained with the
various modified injectors is shown in Figures 17 and 18. The "G"
modification was selected for use in the cluster concept evaluation con-
ducted in Task B, because of its smooth ignition, stable combustion,
performance, heat-transfer and pressure-drop characteristics. Maximum
steady-state chamber pressure oscillations of ±1.7% were exhibited with
this version of the R-14B injector. Combustion efficiency and specific
impulse performance are shown in Figures 19 and 20. The variation in
performance between two of the eight injectors which were used in
evaluating the cluster concept can be seen; this was approximately a 1%
variation. The 17-element coaxial injector exhibits a more uniform flame
front and spray pattern than does the single-element concentric pentad
injector. Consequently, the circumferential heat flux to the chamber
wall is more evenly dispersed, permitting a reduction in the quantity of
film coolant required to conduct duration tests without chamber erosion.
Shown in Figure 21 is a profile of the chamber, the distance between the
film-coolant stations, and the placement of the temperature probes,
designated by "TCW". The axial temperature profile obtained with the
"G" mod R-14B injector-cluster module configuration is shown in Figure 22.
The slight variation in circumferential heat flux was attributed to the
proximity of the injector elements to the thrust chamber wall.

3. Performance Calculations.

(U) a. General. After the raw data were acquired, characteristic
velocity, specific impulse, thrust coefficient, and overall mixture ratio
were calculated. Characteristic velocity was the performance parameter

FUEL MANIFOLD

OXIDIZER MANIFOLD

Seventeen-Element Coaxial Injector

Element Dimensions	R-14B Orig.	Mod"C"	Mod"D"	Mod"E"	Mod"F"	Mod"G"	Mod"H"
a	.290	.375	.375	.375	.375	.375	.375
b	.415	.415	.415	.415	.415	.415	.415
c	.471	.471	.471	.471	.489	.489	.500
d	.125	.200	.125	.125	.125	.125	.125
e	0	1.000	1.000	2.707	2.707	3.207[*]	3.207[*]
f	.290	.290	.290	.304	.304	.375	.375

[*] Total oxidizer tube length is 3.207 inches.

Figure 16. Seventeen-Element Coaxial Injector Modification Chart

(This page is Unclassified)

Figure 17. Percent $C*_{th}$ versus Mixture Ratio, Injector R-14B, Mods. C, D, E, F, and H

Figure 18. Percent I_{sth} versus Mixture Ratio, Injector R-14B, Mods. C, D, E, F, and H

%C*th vs. M.R.

LTE INJECTOR R-14B, MOD G

17 CONCENTRIC ELEMENTS

INJ.	M.R. TEST NO.	
⊙ R-14G-1	175, 176, 177, 178 179, 188, 189	
△ R-14G-2	183, 184, 185	

Figure 19. Percent C*th versus Mixture Ratio, Injector R-14B, Mod. G

Figure 20. Percent I_{sth} versus Mixture Ratio, Injector R-14B, Mod. G

25K FILM-COOLED THRUST CHAMBER, 45L*

SEVENTEEN-ELEMENT COAXIAL INJECTOR, R-14B

Figure 21. Thrust Chamber Wall Temperature Probe Locations

(This page is Unclassified)

Figure 22. Thrust Chamber Wall Temperatures

43

CONFIDENTIAL

of major interest in evaluating and comparing the injector patterns; its
method of calculation is explained below. Specific impulse was calculated
from the equation $I_s = \dfrac{F}{\dot{w}_t}$, and served as a check on the reliability
of the chamber pressure measurements. The thrust coefficient was
calculated from the equation $C_F = \dfrac{F}{PcA_t}$. Actual performances, C^*_a
and I_{s_a}, were calculated and compared with shifting equilibrium
theoretical data curves, derived from an LO_2/LH_2 computer program
formulated by the AFRPL Analysis Section. The thrust coefficient
efficiency was obtained from the equation

$$\%C_{F_{th}} = \frac{\%I_{s_{th_{S.\ L.}}}}{\%C^*_{tn}} \tag{4}$$

to determine nozzle performance. Data-point time slices were
taken during the later half of the test-firing duration. An error analysis
study on data precision was conducted as explained below.

(U) b. Characteristic Velocity. The equation used for
calculating the characteristic velocity was $C^*_a = \dfrac{PcA_t\ g}{\dot{w}_t}$ based on the
total propellant flow rate to the injector-chamber assembly. To render
the parameter more meaningful, treatment of the dependent variables
Pc, A_t, and $\dot{w}_t$ was as follows:

Chamber Pressure, Pc. To measure chamber pressure,
two pressure transducers were installed in parallel from a pressure tap
mounted on the injector-chamber mating flange. If any variation in the
two measurements existed, the average was used and corrected for nozzle
stagnation pressure at the chamber throat. The correction for nozzle
stagnation pressure is a function of the combustion gas specific heat ratio,
γ, and the chamber contraction ratio, ϵ_c. The equations

$$\frac{Pc}{Pcs} = (1 + \gamma M^2_{ni})\left(\frac{1}{1 + \frac{\gamma-1}{2}M^2_{ni}}\right)^{-\frac{\gamma}{\gamma-1}} \tag{5A}$$

CONFIDENTIAL
(This page is Unclassified)

44

$$\text{and} \quad \frac{A_c}{A_t} = \epsilon_c = \frac{1}{M_{ni}} \left(\frac{1 + \frac{\gamma - 1}{2} M_{ni}^2}{\frac{\gamma + 1}{2}} \right)^{\frac{\gamma + 1}{2(\gamma - 1)}} \tag{5B}$$

were used to plot a family of curves, pressure ratio, Pc/Pcs, versus contraction ratio, ϵ_c, maintaining γ constant for a given curve. The momentum of the injected propellants is assumed negligible. An average γ was chosen for the range of mixture ratios investigated. This introduced a maximum error of 0.3% in the accuracy of the nozzle stagnation pressure computation. The correction Pcs = .9485 Pc was used for all firings.

Chamber Throat Area, A_t. The throat area was measured before and after each run. If erosion occurred, several triangulation measurements of the throat contour were taken. The contour was then drawn to scale. The initial throat configuration was superimposed upon the post-run map and the differential area was obtained by integration (summing the squares), and added to the pretest throat area. The change in area was plotted as a linear function of run time (Reference 5). Therefore, for a given data slice at time, t, the area of the throat could be determined.

Flow Rate Measurements. The volumetric measurements were converted to weight flow rate by the equation

$$\dot{w} = \rho \, K \, \text{(cps)} \tag{6}$$

The density, ρ, was determined from pressure and temperature measurements taken at the flowmeter inlet, in conjunction with p-v-t data for LH_2 and LO_2 supplied by the National Bureau of Standards (Reference 6) and the Chemical Propellant Information Agency (Reference 7), respectively. The flowmeter constant, K, was obtained from water-flow calibrations. The cycles per second, cps, were obtained with a magnetic pickup and recorded on FM tape. Cycles were counted over a 200-millisecond interval extending 100 milliseconds before and

after each data point time, t. The actual C* was then compared with the theoretical value and the efficiency was obtained. No correction was made for heat loss to the chamber wall. The correction from actual to nominal chamber pressure was found to be negligible.

(U) c. <u>Film-Coolant Flow Rate.</u> The fuel flow rate to each film-coolant manifold of the thrust chamber module was calculated from the equation

$$\dot{w} = \frac{C_d A}{12} \sqrt{2g\Delta P\rho} \tag{7}$$

where,

A is the area of the individual orifices

C_d is the discharge coefficient determined from water calibration

ΔP is the differential pressure across each orifice obtained by using a specially instrumented manifold, and

ρ is the fuel density determined from p-v-t data and temperature-pressure measurements in the film-coolant manifold.

The film-coolant flow rate through the injector was determined by subtracting the fuel used in film cooling the thrust chamber from the total fuel flow rate. Then, knowing the total injector area for fuel injection and the amount of fuel transported to the injector, a discharge coefficient was calculated which was assumed to be the same for all fuel injection ports. By taking the ratio of film-coolant hole total area to the total fuel injection area and multiplying by the fuel flow rate to the injector, the injector film-coolant flow rate was determined. The fuel used to transpiration-cool the injector faceplate is assumed to be negligible.

(U) d. <u>Thrust.</u> The thrust parameter was measured with a load cell and recorded on an oscillograph. Flexures were installed on both sides of the load cell between the thrust structure and restraining superstructure to compensate for misalignment of axial force.

(U) e. <u>Data Precision</u>. A quality-control study was conducted to determine the precision of the quoted characteristic velocity and specific impulse. Through repetitive calibrations and readings of data, a 95% tolerance interval was established on the various parameters measured. With the above information, and utilizing a method presented in Reference 8, an error analysis was conducted. It was determined that actual values of characteristic velocity and specific impulse were precise within ±1.13% and ±1.37%, respectively, for this task.

SECTION III

TASK B, CLUSTERED-MODULES CONCEPT

A. GENERAL.

(U) A simplified method for clustering discrete thrust chamber assemblies was investigated by clustering eight 25,000-pound thrust, film-cooled modules around a common altitude-compensating, zero-length plug nozzle. Figure 23 shows the cluster assembly which develops 200,000 pounds nominal thrust, installed in the vertical firing position. Prior to the cluster concept demonstration, single-module evaluation was conducted in Task A. In the clustered configuration, the modules were tilted 16 degrees inward from vertical at the nozzle exit such that the exhausting combustion gasses completely enclosed the compensating plug nozzle (see Figure 24). The resulting cluster area ratio, ϵ_{Cl}, was 9.0 as compared to the single-module area ratio, ϵ_M, of 5.5. The cluster design parameters are given in Table III. Propellants were distributed to the cluster by using only a single pair of propellant valves, simplified manifolding, and nonrigid inlet ducts to the injectors. The fuel and oxidizer manifolds were designed to provide even propellant distribution to the injectors. The fuel header manifold is shown in Figure 25 in the center of the inverted partial cluster assembly. Flex joints were provided in the fuel inlet ducts to compensate for thermal contraction due to the cryogenic propellant. Also shown in Figure 25 is the plug nozzle support. The 6-inch oxidizer header manifold with the nonrigid propellant ducting (flex hoses) is pictured in Figure 26. An offshoot tube from each fuel inlet duct was provided to transport liquid hydrogen for film-cooling each module. The film-coolant ducting, shown in Figure 27, consisted of 3/4-inch tubing welded to the fuel ducting upstream of the injector mating flange. Orifices, sized in Task A, were located in the AN fittings of the three chamber coolant manifold inlets to meter the fuel flow to the

48

Figure 23. Cluster Assembly of Eight 25,000-Pound Thrust Chamber Modules

49

Figure 24. Zero-Length Altitude-Compensating Plug Nozzle

TABLE III

(U) 200,000-POUND THRUST CLUSTER DESIGN PARAMETERS

Module Chamber Pressure	800 psia
Module Mixture Ratio (overall)	5.0/1
Thrust (Total)	200,000 lbs
Number of Modules	8
Tilt Angle	16°
Gap Distance/Module Exit Dia., δ/D_E^*	0.03
Module Area Ratio, ϵ_M	5.52
Cluster Area Ratio, ϵ_{Cl}	9.0
Module Design Pressure Ratio	35.7
Cluster Design Pressure Ratio	70.0

*See Figure Below

Figure 25.   Partial Cluster Assembly, Inverted

Figure 26. Six-Inch Oxidizer Header Manifold Assembly

Figure 27. LH_2 Film-Coolant Ducting and Fuel-Header Manifold Support

chamber. Also shown in Figure 27 are turnbuckles for individual module horizontal thrust restraint and the header manifold support consisting of a center post with four legs for vertical and horizontal restraint. Four $\frac{1}{2}$-inch rods for centering the header can also be seen. The four center-post legs were bolted to the baseplate zero-length plug-nozzle support, and the turnbuckles were bolted to individual modules. A closeup of the propellant ducting in the total assembly is shown in Figure 28. Cluster ignition was accomplished by a pyrotechnic igniter (Rocketdyne gas generator igniter PN 650717) employing a burn link for ignition detection. Automatic sequence control circuitry eliminated any propellant flow to the cluster in the event any one of the eight igniters malfunctioned. A typical hot-fire sequence consisted of: a) $1\frac{1}{2}$-hour propellant-line chilldown to insure good quality liquid at the propellant valves on start; b) propellant tanks pressurized; c) electrical impulse sent to igniters; d) ignition detection signal received from igniters; e) fuel propellant valve opened; f) nominal .200-second fuel lead; g) oxidizer propellant valve opened; h) ignition of eight chambers; i) nominal 4-second steady-state test run; j) cutoff; k) oxidizer valve closed; l) 1.000-second fuel lag; m) fuel valve closed. The major data parameters measured in this Task were: total thrust, total propellant flow, individual module chamber pressure, and baseplate temperature and pressure.

B. DESIGN APPROACH.

(U) With the single-module specifications already defined in Task A, the remaining cluster design parameters, cluster area ratio, tilt angle, number of modules, gap distance, and plug length were determined from data obtained in preliminary studies conducted by Pratt and Whitney (see References 9 and 10). The tilt angle, θ_T, is defined as the difference between the Prandtl-Meyer turning angles, ω, of the cluster and module area ratios:

$$\theta_T = \omega_{Cl} - \omega_M \qquad (8)$$

FUEL INLET

FUEL HEADER MANIFOLD

OXIDIZER INLET

INJECTOR-CHAMBER MATING FLANGES

FILM COOLANT OFF SHOOT

Figure 28. Cluster Assembly, Propellant Manifolding and Ducting

56

where

$$\omega_{C1,M} = \sqrt{\frac{\gamma+1}{\gamma-1}} \; \text{Arctan} \sqrt{\frac{\gamma-1}{\gamma+1}(M^2_{C1,M}-1)} - \text{Arctan}\sqrt{M^2_{C1,M}-1}. \quad (9)$$

The cluster area ratio, ϵ_{C1}, which is defined as the ratio of the circular area enclosing all module exits to the sum of the individual module throat areas, is determined by the conventional gas dynamic relationship

$$\epsilon_{C1} = \frac{1}{M_{C1}} \left[\left(\frac{2}{\gamma+1}\right) \left(1 + \frac{\gamma-1}{2}M^2_{C1}\right) \right]^{\frac{\gamma+1}{2(\gamma-1)}} \quad (10)$$

Equation 8 along with the following equation,

$$\frac{\epsilon_{C1}}{\epsilon_M} = \frac{1}{N}\left[\frac{(1+\delta/D_E)\; \text{Cos}\,\Theta_T}{\text{Sin Arctan}\;(\text{Cos}\,\Theta_T \text{Tan}\,180^\circ/N)} + \text{Cos}\,\Theta_T \right]^2, \quad (11)$$

derived from cluster configuration geometric relationships, completely describe a plug cluster nozzle. An approximation of Equation 11 approaches

$$\frac{\epsilon_{C1}}{\epsilon_M} = \frac{1}{N}\left[\frac{(1+\delta/D_E)N}{\pi} + \text{Cos}\,\Theta_T \right]^2, \quad (12)$$

as the number of modules, N, increases. If the ratio (δ/D_E) is assumed to be zero, Equation 12 becomes

$$\frac{\epsilon_{C1}}{\epsilon_M} = \frac{1}{N}\left(\frac{N}{\pi} + \text{Cos}\,\Theta_T\right)^2. \quad (13)$$

Therefore, having a given ϵ_M and γ and using the equations above, one of the three parameters N, ϵ_{C1}, and Θ_T is defined if the other two are arbitrarily chosen.

CONFIDENTIAL

(C) An isentropic plug nozzle axial length is determined by gas
dynamics and cluster geometry. If a full-length plug nozzle is truncated,
its performance decreases. However, Pratt and Whitney determined that
a zero-length plug nozzle would sustain only moderate efficiency losses,
3 to 4%.

C. TEST PROGRAM.

(C) The cluster configuration was evaluated during 13 valid test firings.
The resulting test data is given in Table IV. Combustion efficiency and
specific impulse performance are plotted in Figures 29 and 30. In the
first two test firings with the cluster configuration and R-14B injector,
ignition was readily attained but oxidizer feed system problems were
encountered in the form of low-frequency chugging instability. Initially,
cavitating venturis were included in the design and installed in the oxidizer
feed system between the header manifold and injector inlet ducting, to
prevent any coupling between modules and the propellant feed system.
However, oxidizer feed system pressure limitations permitted only
marginal cavitation conditions to exist in the venturis. Chamber pressure
fluctuations momentarily eliminated cavitation thereby increasing feed
system pressure drop and decreasing the oxidizer flow rate necessary to
maintain design chamber pressure. This situation may have been
amplified by the coaxial injector since low-frequency instability was
experienced in Phase I of the program with a similar injector pattern
when it was tested below design conditions.

(U) The oxidizer feed system problem was resolved by redesigning the
header manifold from the 4-inch configuration shown in Figure 31 to the
6-inch configuration previously shown in Figure 26, and eliminating the
cavitating venturis, thereby reducing the system pressure drop. Also,
from an analysis of historical data, the maximum working pressure of the
run tank was uprated. In the interim, the injector was modified and tested,
as a single module, to improve its operating characteristics as described
in Task A.

58

CONFIDENTIAL

Test No.	v_o ft/sec	ΔP_o psi	ρ_{man} lb/ft³	$\dot{w}_o$ lb/sec	v_f ft/sec	ΔP_f psi	ρ_{man} lb/ft³	$\dot{w}_f$ lb/sec	$\%w_t$ fc ov
		R - 14B	Cluster						
131	99.4	127	60.5	375	451	130	4.32	91.3	4.2
132	102.3	107	61.1	390	564	128	3.97	102.0	4.0
		R - 14G	Cluster						
192	91.6	189	62.7	599	303	124	4.45	77.1	1.51
193	68.7	159	64.8	464	448	190	4.32	107.5	2.02
194	60.7	139	65.1	412	488	219	4.49	121.1	2.33
195	59.3	135	68.7	425	505	215	4.32	120.4	2.22
196	68.4	152	67.3	480	353	172	4.49	89.9	1.99
197	58.5	127	69.4	423	440	216	4.45	109.5	2.30
198	63.1	128	62.6	412	481	207	4.18	111.5	2.24
199	58.9	89.6	68.7	422	659	230	2.87	103.9	1.92
200	56.4	122	67.7	398	454	193	4.54	114.1	2.33
201	55.8	94.6	68.1	396	592	233	3.68	119.5	2.23
202	58.4	100	68.2	415	545	243	4.15	124.7	2.30

v_f ft/sec	ΔP_f psi	$\rho_f$man lb/ft^3	$\dot{w}_f$ lb/sec	$\%w_{t_{fc}}$	M.R. overall	P_{cs} psia	F 10^3lb	A_{t} in^2	C^*_a ft/sec	C^*_{th} ft/sec	$\%C^*_{th}$	Is_a sec	Is_{th} sec
451	130	4.32	91.3	4.2	4.11	536	126	163.5	6060	7952	76.2	271	371
564	128	3.97	102.0	4.0	3.82	571	129	163.5	6110	7982	76.6	262	374
303	124	4.45	77.1	1.51	7.77	764	179.9	163.4	5940	7100	83.7	266	354
448	190	4.32	107.5	2.02	4.32	756	172.3	163.4	6840	7885	87.8	299	379
488	219	4.49	121.1	2.33	3.40	732	171.0	164.2	7250	8005	90.6	321	376
505	215	4.32	120.4	2.22	3.53	735	167.6	164.2	7060	7984	89.1	306	380
353	172	4.49	89.9	1.99	5.34	716	170.1	164.2	6640	7730	85.9	298	373
440	216	4.45	109.5	2.30	3.86	734	167.3	164.2	7280	7980	91.2	314	378
481	207	4.18	111.5	2.24	3.70	709	166.6	164.2	7160	7993	89.6	318	376
659	230	2.87	103.9	1.92	4.06	720	-	164.2	7230	7962	90.8	-	-
454	193	4.54	114.1	2.33	3.49	705	164.0	164.2	7280	8002	91.0	320	375
592	233	3.68	119.5	2.23	3.31	726	164.4	161.8	7330	8002	91.6	319	376
545	243	4.15	124.7	2.30	3.33	751	167.4	161.8	7238	8006	90.4	310	377

2

ST RESULTS

c^*_{th}	Is_a sec	Is_{th} sec	$\%Is_{th}$	$\%CF_{th}$	L^* in	Steady-State Duration sec	Remarks
5.2	271	371	73.0	-	45	.4	Short duration test, chugging instability
5.6	262	374	70.0	-	45	.3	Short duration test, chugging instability
3.7	266	354	75.2	89.8	45	1.8	Slight module chamber erosion, very stable run
7.8	299	379	79.5	90.5	45	5.9	Very smooth transients & steady-state run
0.6	321	376	85.2	94.0	45	3.3	Very smooth transients & steady-state run
9.1	306	380	81.4	91.4	45	3.8	
5.9	298	373	79.9	93.0	45	3.9	First CRG evaluation test, slow gimbal rate
1.2	314	378	83.1	91.1	45	3.9	
9.6	318	376	84.6	94.4	45	3.9	
0.8	-	-	-	-	45	3.9	Load cell flexure failure, no thrust recorded
1.0	320	375	85.3	93.7	45	3.9	
1.6	319	376	84.8	92.6	45	3.8	Modules' horizontal thrust restrained, gimbal rate was still slow
0.4	310	377	82.2	90.9	45	3.8	

%C*th vs. M.R.

CLUSTER OF EIGHT 25K MODULES

INJ.	TEST NO.
R-14B	131, 132
R-14B, Mod G	192, 193, 194, 195, 196
	197, 198, 199, 200, 201, 202

M.R.(overall)

Figure 29.   Percent C*th Versus Mixture Ratio, Clustered Configuration

Figure 30. Percent I_{sth} Versus Mixture Ratio, Clustered Configuration

Figure 31. Four-Inch Oxidizer Header Manifold with Cavitating Venturi

63

(This page is Unclassified)

CONFIDENTIAL

(C) The cluster evaluation was then resumed at design conditions and no feed system problems were experienced during 11 subsequent 4-second test firings. Very smooth start and cutoff transients were obtained with the simplified propellant manifolds and all eight modules primed within 80 milliseconds. A representative start transient of a cluster firing is shown in Figure 32. PC-1A through PC-8A identify the individual module chamber pressure traces. Chamber pressure variations between modules was approximately ±2.5% from the mean. The peak-to-peak pressure oscillations of the particular modules varied from ±1.2 to ±1.6% of steady-state chamber pressure.

(C) The majority of the tests were conducted at relatively low overall mixture ratios (3.3/1 to 4/1, injector end mixture ratios of 3.7/1 to 4.5/1, respectively) in order to adequately demonstrate the cluster concept without suffering the greater performance losses due to film cooling at higher mixture ratios as determined under Task A. One test firing was inadvertently conducted at an overall mixture ration of 7.8/1 due to a readout error in flow-rate measurement from previous cold-flow tests. The error was recognized and corrected prior to the next hot firing.

(C) The combustion efficiency obtained with the cluster modules compared closely with that obtained during the single-module tests of Task A, as was expected. Variations are attributed to performance differences and quality control of experimental components, and instrumentation accuracy of the two test-firing positions.

(C) The zero-length plug nozzle, as shown in Figure 24, consisted of an eight-pointed star-plate. The star points are tilted 16° from horizontal to fair flush with individual modules at their nozzle exits. The plate was instrumented for pressure and temperature sensing on the flame side. Figure 33 gives location of the pressure transducers and a typical graph of nondimensional baseplate pressure versus radial distance from the plate center for test number 197. Average baseplate pressure varied from 27.6 psia to 23.1 psia for the tests conducted as indicated in Table V.

CONFIDENTIAL

TIMING

←—0.100 SEC.—→

LO₂ START VALVE CLOSED
LO₂ START VALVE OPEN
LH₂ START VALVE CLOSED

IGNITER FIRE SWITCH — LH₂ START VALVE OPEN
RCC CUTOFF
PC-4A

IGNITION DETECTION SIGNAL

PC-8A
PC-6A
PC-1A
LO₂ TANK PRESSURE — CUTOFF GENERAL
CENTER REFERENCE

PC-5A
PC-3A
PC-2A
LH₂ TANK PRESSURE
PC-7A
LO₂ FEED LINE PRESSURE
LH₂ FEED LINE PRESSURE

F-1(THRUST)
LO₂ START VALVE POSITION
LH₂ START VALVE POSITION

(U) FIGURE 32 - OSCILLOGRAPH TRACE HOT FIRE 194 START TRANSIENT

VAL'E OPEN

GENERAL

LLOGRAPH TRACE HOT FIRE 194 START TRANSIENT

2

Figure 32. Oscillograph Trace, Hot Fire 194 Start Transient

Figure 33. Plug Nozzle Pressure versus Transducer Location,
Zero-Length Plug Nozzle, HF-197

(C) TABLE V ZERO-LENGTH PLUG NOZZLE TEST RESULTS

Run No.	PB-1 psia	PB-2 psia	PB-3 psia	PB-4 psia	PB-5 psia	PB-6 psia	PB-7 psia	PB-8 psia	PB-9 psia	Pcq psia	PE Ave psia	PBave Pcs	%Is Us.L	%CF	M.R. Overall	PBave/PA	Pcr/PA
			Injector R - 14B Cluster														
131	23.1	19.22	17.26	19.52	19.23	18.82	-	-	-	536	19.53	.0364	73.0	-	4.11	1.495	41.0
132	22.3	19.80	18.23	20.3	20.4	19.33	-	-	-	571	20.1	.0352	70.0	-	3.82	1.536	43.6
			Injector R - 14G Cluster														
192	28.7	29.1	25.6	28.7	28.0	25.6	-	-	-	764	27.6	.0362	75.2	89.8	7.77	2.108	58.4
193	28.6	27.4	24.6	26.1	27.5	25.4	-	-	-	756	26.6	.0352	79.5	90.5	4.32	2.032	57.7
194	25.2	25.1	23.8	27.1	25.0	24.2	24.6	23.3	28.1	732	25.2	.0344	85.2	94.0	3.40	1.947	56.6
195	26.1	25.7	24.3	26.3	25.0	24.3	25.4	23.5	26.9	735	25.3	.0344	81.4	91.4	3.53	1.920	55.8
196	-	26.2	24.5	27.2	26.0	24.6	26.6	23.6	28.3	716	25.9	.0362	79.9	93.0	5.34	1.964	54.3
197	26.4	25.2	23.3	26.2	25.2	24.4	25.2	22.7	24.6	734	24.8	.0338	83.1	91.1	3.86	1.884	55.8
198	26.0	24.9	22.1	24.7	24.4	22.6	25.0	21.9	23.8	719	24.0	.0334	84.6	94.4	3.70	1.823	54.6
199	26.9	25.8	24.5	26.3	25.0	24.1	25.3	22.8	24.4	720	25.0	.0347	-	-	4.06	1.904	54.8
200	25.7	23.4	23.6	25.0	23.9	22.8	24.5	21.7	23.4	705	23.7	.0336	85.3	93.7	3.49	1.793	53.7
201	24.0	23.3	19.8	28.5	23.5	23.3	22.7	21.1	21.9	726	23.1	.0318	84.8	92.6	3.31	1.748	55.0
202	25.9	24.6	20.3	29.8	25.4	23.8	24.5	22.0	23.1	751	24.4	.0325	82.3	90.9	3.33	1.847	56.8

The nondimensional baseplate pressure data, PB/P_A, correlates within 5% of cold-flow data obtained on an independent research and development program conducted by Pratt and Whitney Aircraft (Reference 11) on a model simulating the Scorpio cluster configuration and its tilt angle (see Figure 34). Pratt and Whitney determined that the isentropic tilt angle for the Scorpio cluster and the LO_2/LH_2 propellant combination should be 9.3°. A comparison of nozzle performance for the 9.3° and 16° tilt angle is shown in Figure 35.

(C) The average temperatures measured on the plug plate varied from $467^\circ F$ to $1050^\circ F$, depending on the location of the probe. As shown in Figure 36, higher temperatures were obtained on a radial line intersecting the centerline of a module than were obtained on a radial line passing through a star point. The refractory coating used as a thermal barrier for the inside walls of the modules was also coated on the plug plate's flame side. Discoloration and some flaking of the coating was noted in the course of the 13 hot-fire tests, but no erosion of the plate was experienced. The maximum recorded temperatures for the last nine 4-second tests varied from 1160° to $1540^\circ F$.

(C) The thrust coefficient performance obtained from hot-fire tests with the cluster is shown in Figure 37. Here again, this agrees within 5% of the cold-flow data obtained by Pratt and Whitney on the 16° tilt angle model. When the cluster was hot-fired very near the module design conditions of 700 psia chamber pressure and 4/1 overall mixture ratio, 94.4% $C_{F_{th}}$ was obtained which is almost in exact agreement with the cold-flow data. The thrust coefficient and specific impulse performance obtained with the cluster are lower than those obtained during the single-module tests. This is probably due to frictional or shock losses incurred by intersecting exhaust plumes, and larger than isentropic tilt angle. The items cited for combustion efficiency variations, that is, performance differences and quality control of experimental components and instrumentation accuracy of the two test-firing positions, may also impose their influence on thrust coefficient and specific impulse variations.

Figure 34. Hot-Fire and Cold-Flow Baseplate Pressure Correlation

Figure 35.   Tilt-Angle Effect on Nozzle Performance,   Zero-Length Plug

73

TEST NO. 194, 195, 196, 197, 198, 199, 200, 201, 202

MAXIMUM 1170, 1240, 1500, 1370, 1370, 1540, 1340, 1160, 1260
TEMPERATURE
RECORDED

Figure 36. Plug Nozzle Temperature Data

%CF$_{th}$ vs. M.R.

CLUSTER OF EIGHT 25K MODULES

INJECTOR R-14B, MOD. G

Figure 37. Percent CF$_{th}$ versus Mixture Ratio, Clustered Configuration

D. PERFORMANCE CALCULATIONS.

(U) 1. General.

Performance calculations for Task B were the same as those for Task A except for the changes cited below. An error analysis was conducted on data precision for this Task and it was determined that the actual values of characteristic velocity and specific impulse were precise within ±2.10 and ±2.01, respectively. A typical instrumentation specification list is included in the Appendix. The instrumentation techniques and recording methods were the same as those presented in the Phase I final report, AFRPL-TR-65-149 (Reference 1).

(U) 2. Chamber Pressure, Pc.

To measure cluster chamber pressure, two pressure transducers were mounted on the chamber-injector mating flange of each module. Unless any transducer recording varied by more than 5% from the mean, the average of all the pressures was corrected for nozzle stagnation pressure at the chamber throat. The correction for nozzle stagnation pressure is a function of the combustion gas specific heat ratio, γ, and the chamber contraction ratio, ϵ_c, and was the same as described in Task A.

(U) 3. Throat Area, A_t.

The throat area used was a summation of the individual module throat areas. Any throat area change due to erosion was determined as described in Task A.

(U) 4. Propellant Flow Rate, $\dot{w}$.

With the exception of a 12-inch turbine flowmeter used to measure LH_2 flow for the cluster (as opposed to Task A's 6-inch flowmeter) the method used to determine total propellant flow rate was the same as in Task A.

SECTION IV

TASK C, CAM RING GIMBAL

A. DESCRIPTION.

(U) A unique rocket engine thrust vector control mechanism, called the Cam Ring Gimbal (CRG), was tested during the last seven cluster tests for evaluation under actual hot-fire conditions. Designed by Rocketdyne according to the specifications given in Table VI, the CRG was fabricated and functionally dead-weight-tested under Contract AF 04(611)-8192 (Reference 12). The mechanical assembly consisted of four hollow rings mounted vertically in line--an upper stationary wedge-shaped ring for vehicle attachment, two movable wedge-shaped rings, and a lower stationary ring for engine attachment. Figure 38 shows the CRG assembled in place of the simulation ring previously shown in Figure 23. The desired thrust vector angle, to a maximum of $\pm5^{\circ}$ in any direction, can be obtained by rotating the two movable wedges relative to or with each other. The assembled ring dimensions are 18 inches in height and 50 inches in diameter.

(U) Each cam ring is independently rotated; therefore, with variable drive actuators, change from one thrust vector angle to another can be accomplished directly without any circular motion of the gimbal angle. For demonstration purposes, the gimbal's two movable wedges were actuated through gear drive by the two 10-horsepower electric motors shown in Figure 39. Since the gimbal mechanism is prototype, a simplified control system was used which allowed only one predetermined gimbal cycle per cluster test. A typical cycle consisted of: a) start from 0° pitch, 0° yaw; b) gimbal to $+5^{\circ}$ pitch, 0° yaw; c) reverse to -5° pitch, 0° yaw and stop. Electrical signals from a rotary potentiometer located on each actuator drive shaft were recorded on an oscillograph to

TABLE VI

CAM RING GIMBAL, DESIGN SPECIFICATIONS

Thrust	200,000 lbs
Angular Displacement	$\pm 5^{\circ}$
Gimbal Rate	10° per sec
Gimbal Acceleration	1 rad per sec^2
Horsepower required per actuator	10
Voltage	220 AC/440 AC
Max. Angular Velocity of either cam ring	115°/sec

Figure 38. Cam Ring Gimbal, Cluster Assembly

Figure 39. Cam Ring Gimbal with Actuators

give a time trace of the cycle. The potentiometer signals for each ring were also paralleled to visual meters shown on the CRG control panel in Figure 40. Three electrical power supplies were used for CRG actuation and control. The electric motor actuators were powered by either 220 or 440 v. a. c. The actuator power was controlled by 115 v. a. c. relays located on the test stand, and were in turn operated by 28 v. d. c. relays in the CRG control panel. Depending on the control panel switch settings, the wedges could be inched individually or rotated together (see Figure 41). After start of the gimbal cycle, reverse and stop motion were accomplished by actuation of 28 v. d. c. microswitches located on the gimbal actuator motor mounts. Trip plates (ramps) for microswitch actuation were located on the gears attached to the movable wedges. The positioning of these plates and the actuators' direction of rotation on start determined the angular displacement and direction of the gimbal cycle. Nonrigid propellant ducting, to provide for thrust vectoring, was routed through the available space in the hollow center of the CRG. No internal thrust structure was needed, as the thrust load is transmitted through the gimbal mechanism. The ball bearings and integral raceways between the rings were so designed as to withstand the thrust, side, and hanging loads of the 200, 000-pound thrust, clustered assembly. The clustered assembly is prevented from rotating about its vertical axis by two diametrically opposed ball-link devices hinged to each other and to the upper and lower stationary rings.

B.   TEST RESULTS.

(C) Before being subjected to hot-fire conditions, the CRG was functionally tested with the static hanging load of the cluster assembly and also "inch"-actuated during cold-flow tests. The gimbal rate and response appeared normal under the relatively small applied loads. Figure 42 is a typical gimbal cycle trace from one of the seven hot-fire tests. Shown is the cycle sequence, the total thrust experienced, and the gimbal angle at given intervals. The first 2 of the 10 sequence traces, U (upper ring)

Figure 40. Cam Ring Gimbal Position Meters

82

Figure 41. Cam Ring Gimbal Control Console

(This page is Unclassified)

Figure 42. Cam Ring Gimbal Test Results, Hot Fire 200

PREP and L (lower ring) PREP, indicate total time electric power was available to motor direction relay switches. U+ through L- indicate the direction that the relays actuated, e. g., at start, the U+ and L+ relays were energized, and the actuators were initially powered in the +(clockwise) direction for positive pitch thrust vectoring. U REV and L REV indicate the time during which the reverse microswitches were energized. U STOP and L STOP are traces of the stop microswitch actuations. The desired gimbal sequence from start at 0° was a positive 4.5^O pitch, reverse to a negative 4.5^O pitch, and stop. The gimbal motion was to describe a straight line. The actual path of travel approximated a spiral and culminated at a gimbal angle of -6° pitch, 0° yaw. The gimbal angle at given intervals is shown in Figure 42. A 1.5^O overtravel beyond the stop point was experienced, since no dynamic braking was available. A gimbal rate of 2 degrees per second was achieved during steady-state thrust for each of the seven hot-fire tests as compared to the design rate of 10 degrees per second. However, on cutoff, after thrust decayed below 120,000 pounds, the gimbal rate increased to 13 degrees per second. The angular acceleration and velocity of the two rings were different, as evident in Figure 42. Because of the slow gimbal rate and the irregular motion, three major areas of concern were investigated to insure that the CRG was being properly evaluated. These were: (1) electrical power to the actuators; (2) ball bearings and race condition; and (3) distortion of the mechanism due to the horizontal thrust component of the modules' 16° tilt angle. Instrumentation was provided to determine motor power which was found to be within specifications under load conditions. Inspection of the ball bearings and races between firings revealed no deterioration. The turnbuckle bracing shown in Figure 27 was installed to counteract the horizontal thrust component of the individual modules, allowing only the modules' vertical thrust component to be transferred to the gimbal mechanism. Data analysis from the two subsequent hot-fire tests revealed no change in the CRG operation. It appears that the CRG was binding due to structural distortions caused by the total thrust load and/or by thrust variation between individual thrust chamber modules.

SECTION V

SUMMARY

(U) Task A. A total of 44 hot firings were conducted on two 25,000-pound thrust simplified injectors utilizing a 45L* film-cooled thrust chamber. The injector configurations were a single-element concentric pentad and a 17-element coaxial pattern. The following information was obtained:

1. Eight hot firings were conducted on the single-element concentric pentad injector. As was experienced in Phase I with a similar 50,000-pound thrust injector pattern, localized hot spots appeared on the thrust chamber wall in the areas of spray fan impingement, 90° apart. The erosion sustained with the smaller, 25,000-pound thrust chamber was greater than was experienced with the larger 50,000-pound thrust chamber, and is attributed to the volume-to-surface area relationship. Additional film coolant was provided in the areas of spray fan impingement which alleviated the erosion problem. By modifying the injector to include recessed oxidizer tubes from the fuel annuli exit plane, a more uniform spray pattern resulted and performance increased.

2. Thirty-six test firings were conducted on the 17-element coaxial injector. A moderate program of injector modification and chamber film-coolant redistribution and quantity change was pursued to obtain a module which could be used to adequately evaluate the cluster configuration. An interaction in the form of hydraulic orificing was experienced between the oxidizer and fuel ports of each element with this injector. Due to the more uniform spray characteristics, heat flux to the thrust chamber wall was more evenly distributed, thus contributing to reduce the film-coolant requirement to prevent thrust chamber erosion. A general relationship between combustion efficiency and quantity of film coolant was obtained as a function of mixture ratio. With this injector and the previous one, afterburning in the nozzle was evident and was

attributed to incomplete combustion of the film-coolant fuel in the chamber. Neither of the two injectors evaluated under this Phase achieved the high performance obtained with their Phase I counterparts. However, a smooth starting and extremely stable injector ultimately evolved from this portion of the Phase III effort.

(U) Task B. Thirteen valid evaluation tests were conducted on a 200,000-pound thrust, simplified cluster concept for thrust chamber modules. Only two propellant valves were used for the entire cluster of modules which incorporated a zero-length, altitude-compensating plug nozzle. A simplified propellant feed system was designed which demonstrated stable characteristics. Smooth start and cutoff transients were experienced throughout the investigation. Hot-fire data obtained on the plug nozzle correlated with 5% of cold-flow data obtained from tests on a model simulating the cluster configuration.

(U) Task C. An advanced thrust vector mechanism, the Cam Ring Gimbal, was evaluated under hot-firing conditions during the last seven cluster tests of Task B. At full thrust, the gimbal rate was below its design rate, and the path of travel deviated from that which was programmed. Overtravel was experienced at the return and stop gimbal angles.

SECTION VI

CONCLUSIONS

(C) Based on the data obtained from the evaluation tests conducted under the various tasks of this Phase III effort, the following conclusions were made:

(C) <u>Task A.</u> Simplified injectors can be feasibly used with film-cooled thrust chambers. The spray pattern of the injector has a marked effect on the amount of fuel required to cool the thrust chamber. The more evenly the heat flux is distributed, the more efficiently the coolant can be utilized, thus decreasing the coolant quantity required to prevent erosion. The quantity and distribution of the film coolant and mixture ratio influences the performance of the injector-chamber assembly. Comparing the uncooled test results from Phase I with the similar injector patterns evaluated under this task, it appears that approximately $2\frac{1}{2}\%$ combustion performance loss can be attributed to both film-cooling and chamber L^* effects. Afterburning can result in the nozzle if the film coolant is not thoroughly combusted in the thrust chamber.

(C) <u>Task B.</u> A simplified clustering technique for thrust chamber modules has been demonstrated in that only two propellant valves were used for the entire cluster of eight 25,000-pound thrust modules which incorporated a zero-length, altitude-compensating plug nozzle. A simplified and stable-flow feed system can be provided to supply propellants to a multi-module configuration to attain high thrust. The number and thrust level of the modules to which the cellular combustor concept can be extended was beyond the scope of this program. Positive pressures, which augment the thrust, can be obtained on a zero-length plug nozzle. Nozzle performance is degraded if the tilt angle of the modules is nonisentropic.

Also, it appears that nozzle performance losses are sustained from the intersection and interaction of module exhaust plumes due to frictional and shock phenomena. It has been verified that cold-flow models can be employed to simulate hot-fire conditions of the cluster nozzle configuration which was evaluated.

(C) Task C. The Cam Ring Gimbal thrust vectoring mechanism was demonstrated feasible under actual hot-firing conditions with the cluster concept. It appeared that structural binding was experienced due to the total thrust load or variation in thrust among the modules. Further development, with regard to gimbal rate and travel path control. is required to improve its operation.

APPENDIX

TYPICAL INSTRUMENTATION SPECIFICATION LIST

INSTRUMENTATION SPECIFICATION SHEET

PROJECT 305B02305 SHEET 1 OF 10

TEST NUMBER

PROJECT TITLE   DATE

SCORPIC-8 ENG CLUSTER, TS1-5A   NOV 1984

ITEM NR. PARAMETER		LOCATION	TRANSDUCER TYPE	TRANS. RANGE	CAL. RANGE	FREQ.RANGE	REC.SYS.	CHANNEL
1	POT-1	OX TANK	WIANCKO	0-2000 PSIG	0-1500	1 CPS	L+N	15A
2	POT-2	OX TANK	WIANCKO	0-2000 PSIG	0-1500	1 CPS	L+N VSUAL	15B
3	PFT-1	FUEL TANK	WIANCKO	0-2000 PSIG	0-1500	1 CPS	L+N	16A
4	PFT-2	FUEL TANK	WIANCKO	0-2000 PSIG	0-1500	1 CPS	L+N VSUAL	16B
5	POTR	OX PRES REG	WIANCKO	0-2000 PSIG	01500	1 CPS	L+N VSUAL	15C
6	PFTR	FUEL PRES REG	WIANCKO	0-2000 PSIG	0-1500	1 CPS	L+N VSUAL	16C
7	PORL	OX REG PRESLINE	WIANCKO	0-2000 PSIG	0-1500	1 CPS	METER	
8	PFRL	FUELREG PRESLINE	WIANCKO	0-2000 PSIG	01500	1 CPS	METER	
9	POMP	OX MAN PUR	WIANCKO	0-750 PSIG	0-600	1 CPS	METER	
10	PFMP	FUEL MAN PUR	WIANCKO	0-750 PSIG	0-600	1 CPS	METER	
11	PGHI	GH2 CASCADE	WIANCKO	0-7000 PSIG	0-6500	1 CPS	L+N	14B
12	PGHP	GH2 MAN	WIANCKO	-7000 PSIG	0-6500	1 CPS	METER	
13	PGNT	GN2 CASCADE	WIANCKO	0-7000 PSIG	0-6500	1 CPS	L+N	14A
14	PGNP	GN2 MAN	WIANCKO	C-7000 PSIG	0-5000	1 CPS	METER	
15	PGNS	GN2CROSSCOUNTRY	WIANCKO	0-7000 PSIG	0-6500	1 CPS	M T	
16	TOT	OX TANK	WIANCKO-DIFF	-20 PSIG		PS	L+N	15C

INSTRUMENTATION SPECIFICATION SHEET   SHEET 2 OF 10   TEST NUMBER   PROJECT TITLE   DATE

PROJECT 305802305   SCORPIO-8 ENG CLUSTER, TSI-5A   NOV 1964

ITEM NR.	PARAMETER	LOCATION	TRANSDUCER TYPE	TRANS. RANGE	CAL. RANGE	FREQ. RANGE	REC.SYS.	CHANNEL
31	TOLFT-1	FUEL TANK	RTB	RANGE 97	-435-335 OF	1 CPS	L+N	77B
32	TOLFT-2	FUEL TANK	RTB	RANGE 97	-435-335 OF	1 CPS	L+N	
33	TOLFT-3	FUEL TANK	RTB	RANGE 97	-435-335 OF	1 CPS	L+N	
34	TOLFT-4	FUEL TANK	RTB	RANGE 97	-435-335 OF	1 CPS	L+N	
35	TOLFT-5	FUEL TANK	RTB	RANGE 97	-435-335 OF	1 CPS	L+N	78B
41	ENGINE START	EA NO 36	SWITCH			60 CPS	OSC TAPE	M7
42	CUTOFF RCC	EA NO 30	SWITCH			60 CPS	OSC TAPE	M8
43	CUTOFF GENERAL	EA NO 11	SWITCH			60 CPS	OSC TAPE	M19
44	FUEL START OPEN	EA NO 34	SWITCH			60 CPS	OSC TAPE	M5
45	FUEL START CLOSED	EA NO 33	SWITCH			60 CPS	OSC TAPE	M4
46	OX START OPEN	EA NO 32	SWITCH			60 CPS	OSC TAPE	M3
47	OX START CLOSED	EA NO 31	SWITCH			60 CPS	OSC TAPE	M2
48	IGN PC-ARM	EA NO 37	SWITCH			60 CPS	OSC	C14
61	BASE TIMING	1 P/S					L+N	ALL
62	BASE TIMING	107 PPS					CSC	ELL
63	TAPE TIMING	CPC-LOCK					TAPE	-7

INSTRUMENTATION SPECIFICATION SHEET

PROJECT 305802305   SHEET 3 OF 10

PROJECT TITLE   DATE

SCORPIO-8 ENG CLUSVER, TS1-5A   NOV 1964

TEST NUMBER

ITEM NR.	PARAMETER	LOCATION	TRANSDUCER TYPE	TRANS. RANGE	CAL. RANGE	FREQ.RANGE	REC.SYS.	CHANNEL
64	10 KCPS REF						TAPE	T-2

INSTRUMENTATION SPECIFICATION SHEET

PROJECT 305802305   SHEET 4 OF 10

TEST NUMBER   PROJECT TITLE   DATE

SCORPIO-8 ENG CLUSTER, TSI-5A   NOV 1964

ITEM NR.	PARAMETER	LOCATION	TRANSDUCER TYPE	TRANS. RANGE	CAL. RANGE	FREQ. RANGE	REC. SYS.	CHANNEL
301	PC-1A	INJ 1 FLANGE	STRAIN GAGE	0-1500 PSIG	0-1000	135 CPS	OSC	
302	PC-2A	INJ 2 FLANGE	STRAIN GAGE	0-1500 PSIG	0-1000	135 CPS	OSC	
303	PC-3A	INJ 3 FLANGE	STRAIN GAGE	0-1500 PSIG	0-1000	135 CPS	OSC	
304	PC-4A	INJ 4 FLANGE	STRAIN GAGE	0-1500 PSIG	0-1000	135 CPS	OSC	
305	PC-5A	INJ 5 FLANGE	STRAIN GAGE	0-1500 PSIG	0-1000	135 CPS	OSC	
306	PC-6A	INJ 6 FLANGE	STRAIN GAGE	0-1500 PSIG	0-1000	135 CPS	OSC	
307	PC-7A	INJ 7 FLANGE	STRAIN GAGE	0-1500 PSIG	0-1000	135 CPS	OSC	
308	PC-8A	INJ 8 FLANGE	STRAIN GAGE	0-1500 PSIG	0-1000	135 CPS	OSC	
309	PC-1B	INJ 1 FLANGE	STRAIN GAGE	0-1500 PSIG	0-1000	1 CPS	L+N	9A
310	PC-2B	INJ 2 FLANGE	STRAIN GAGE	0-1500 PSIG	0-1000	1 CPS	L+N	9B
311	PC-3B	INJ 3 FLANGE	STRAIN GAGE	0-1500 PSIG	0-1000	1 CPS	L+N	9C
312	PC-4B	INJ 4 FLANGE	STRAIN GAGE	0-1500 PSIG	0-1000	1 CPS	L+N	10A
313	PC-5B	INJ 5 FLANGE	STRAIN GAGE	0-1500 PSIG	0-1000	1 CPS	L+N	10B
314	PC-6B	INJ 6 FLANGE	STRAIN GAGE	0-1500 PSIG	0-1000	1 CPS	L+N	10C
315	PC-7B	INJ 7 FLANGE	STRAIN GAGE	0-1500 PSIG	0-1000	1 CPS	L+N	11A
316	PC-8B	INJ 8 FLANGE	STRAIN GAGE	0-1500 PSIG	0-1000	1 CPS	L+N	11B

INSTRUMENTATION SPECIFICATION SHEET

PROJECT 305802305   SHEET 5 OF 10   TEST NUMBER

PROJECT TITLE   SCORPIO-A ENG CLUSTER, TS1-5A   DATE NOV 1964

ITEM NR.	PARAMETER	LOCATION	TRANSDUCER TYPE	TRANS. RANGE	CAL. RANGE	FREQ. RANGE	REC. SYS.	CHANNEL
317	PC-1C		PHOTOCON	0-2000 PSIG	0-1000	2100 CPS	TAPE	
318	PC 2C		PHOTOCON	0-2000 PSIG	0-1000	2100 CPS	TAPE	
319	PC 3C		PHOTOCON	0-2000 PSIG	0-1000	2100 CPS	TAPE	
320	PC 4C		PHOTOCON	0-2000 PSIG	0-1000	2100 CPS	TAPE	
325	POM-1	OX MANIFOLD 1	STRAIN GAGE	0-2000 PSIG	0-1000	135 CPS	OSC	P2
326	POM-2	OX MANIFOLD 2	STRAIN GAGE	0-2000 PSIG	0-1000	135 CPS	OSC	P4
327	POM-3	OX MANIFOLD 3	STRAIN GAGE	0-2000 PSIG	0-1000	135 CPS	OSC	P6
328	POM-4	OX MANIFOLD 4	STRAIN GAGE	0-2000 PSIG	0-1000	135 CPS	OSC	P8
329	POM-5	OX MANIFOLD 5	STRAIN GAGE	0-2000 PSIG	0-1000	135 CPS	OSC	P10
330	POM-6	OX MANIFOLD 6	STRAIN GAGE	0-2000 PSIG	0-1000	135 CPS	OSC	P12
331	POM-7	OX MANIFOLD 7	STRAIN GAGE	0-2000 PSIG	0-1000	135 CPS	OSC	P14
332	POM-8	OX MANIFOLD 8	STRAIN GAGE	0-2000 PSIG	0-1000	135 CPS	OSC	P16
333	PFM-1	FUEL MANIFOLD 1	STRAIN GAGE	0-2000 PSIG	0-1000	135 CPS	OSC	P20
334	PFM-2	FUEL MANIFOLD 2	STRAIN GAGE	0-2000 PSIG	0-1000	135 CPS	OSC	P24
335	PFM-3	FUEL MANIFOLD 3	STRAIN GAGE	0-2000 PSIG	0-1000	135 CPS	OSC	P26
336	PFM-4	FUEL MANIFOLD 4	STRAIN GAGE	0-2000 PSIG	0-100	1.5 CPS	OSC	P28

INSTRUMENTATION SPECIFICATION SHEET   TEST NUMBER   PROJECT TITLE   DATE

PROJECT 305802305   SHEET 6 OF 10   SCORPIO-8 ENG CLUSTER, YS1-5A   NOV 1964

ITEM NR.	PARAMETER	LOCATION	TRANSDUCER TYPE	TRANS. RANGE	CAL. RANGE	FREQ.RANGE	REC.SYS.	CHANNEL
337	PFM-5	FUEL MANIFOLD 5	STRAIN GAGE	0-2000 PSIG	0 1000	135 CPS	OSC	P30
338	PFM-6	FUEL MANIFOLD 6	STRAIN GAGE	0-2000 PSIG	0-1000	135 CPS	OSC	P32
339	PFM-7	FUEL MANIFOLD 7	STRAIN GAGE	0-2000 PSIG	0-1000	135 CPS	OSC	P34
340	PFM-8	FUEL MANIFOLD 8	STRAIN GAGE	0-2000 PSIG	0-1000	135 CPS	OSC	P36
341	PICP-1	IGNITOR CHAM 1	WIANCKO	0-2000 PSIG	0-1000	50 CPS	OSC	QL
342	PICP-2	IGNITOR CHAM 2	WIANCKO	0-2000 PSIG	0-1000	50 CPS	OSC	QL
343	PICP-3	IGNITOR CHAM 3	WIANCKO	0-2000 PSIG	0-1000	50 CPS	OSC	QL
344	PICP-4	IGNITOR CHAM 4	WIANCKO	0-2000 PSIG	0-1000	50 CPS	OSC	QL
345	PICP-5	IGNITOR CHAM 5	WIANCKO	0-2000 PSIG	0-1000	50 CPS	OSC	QL
346	PICP-6	IGNITOR CHAM 6	WIANCKO	0-2000 PSIG	0-1000	50 CPS	OSC	QL
347	PICP-7	IGNITOR CHAM 7	WIANCKO	0-2000 PSIG	0-1000	50 CPS	OSC	QL
348	PICP-8	IGNITOR CHAM 8	WIANCKO	0-2000 PSIG	0-1000	50 CPS	OSC	QL
349	POL-1	OX LINE D	WIANCKO	0-2000 PSIG	0-1500	1 CPS	L+N	12A
350	POK-2	OX LINE U	WIANCKO	0-2000 PSIG	0-1500	50.1 CPS	OSC L+N	M49 128
351	POL-3	OX SPIDER	WIANCKO	0-2000 PSIG	0-1500	1 CPS	L+N	11C
352	PFL-1	FUEL LINE C	WIANCKO	0-2000 PSIG	0-1500	1 CPS	L+N	17A

INSTRUMENTATION SPECIFICATION SHEET

PROJECT TITLE   TEST NUMBER   DATE

PROJECT 30502305   SHEET 7 OF 10   SCORPIO-8 ENG CLUSTER, TS1-5A   NOV 1964

ITEM NR.	PARAMETER	LOCATION	TRANSDUCER TYPE	TRANS. RANGE	CAL. RANGE	FREQ.RANGE	REC.SYS.	CHANNEL
353	PFL-2	FUEL LINE U	WIANCKO	0-2000 PSIG	0-1500	50, 1 CPS	OSC L+N	MSO 17B
354	PFL-3	FUEL SPIDER	WIANCKO	C-2000 PSIG	0-1500	1 CPS	L+N	17C
355	PFC-1	FILM COOL LINE	WIANCKO DIF	0-150 PSID	0-100	1 CPS	L+N	74A
356	PFC-2	FILM COOL LINE	WIANCKO DIF	0-150 PSID	0-100	1 CPS	L+N	74D
357	PFC-3	FILM COOL LINE	WIANCKO DIF	0-150 PSID	0-100	1 CPS	L+N	16C
358	PB-1	BASE PLATE	WIANCKO DIF	0-20 PSID	-5+15	1 CPS	L+N	72A
359	PB-2	BASE PLATE	WIANCKO DIF	0-20 PSID	-5+15	1 CPS	L+N	72B
360	PB-3	BASE PLATE	WIANCKO DIF	0-20 PSID	-5+15	1 CPS	L+N	72C
361	PB-4	BASE PLATE	WIANCKO DIF	0-20 PSID	-5+15	1CPS	L+N	73A
362	PB-5	BASE PLATE	WIANCKO DIF	0-20 PSID	-5+15	1 CPS	L+N	73B
363	PB-6	BASE PLATE	WIANCKO DIF	0-20 PSIC	-5+15	1 CPS	L+N	73C
371	TOF	CX MAN	RTB	RANGE 96	-335-245	1 CPS	L+N	7+A
372	TFH	FUEL MAN	RTB	RANGE 47	--35-345 OF	1 CPS	L+N	
373	TCL-1	OX LINE-C	RTB	RANGE 3	-3.5-355 OF	1 CPS	L+N	74A
374	TCL-2	OX LINE-?	-19	RANGE 36			L+?	
375	TCL-1	OX LINE 1	RTB				L+?	74C

INSTRUMENTATION SPECIFICATION SHEET   SHEET 8 OF 10

PROJECT 305002305   TEST NUMBER   PROJECT TITLE   DATE

SCORPIO-8 ENG CLUSTER, TSI-5A   NOV 1964

ITEM NO.	PARAMETER	LOCATION	TRANSDUCER TYPE	TRANS. RANGE	CAL. RANGE	FREQ.RANGE	REC.SYS.	CHANNEL
376	TFL-2	FUEL LINE-U	RTB	RANGE 97	-435-335 DF	1 CPS	LOW	77A
377	TFS	FUEL SPIDER	RTB	RANGE 97	-435-335	1 CPS	LOW	75C
378	TCH-1	CHAM WALL	C/A THERMOCOUPLE		0-2200 DF	1 CPS	LOW	3A
379	TCH-2	CHAM WALL	C/A THERMOCOUPLE		0-2200 DF	1 CPS	LOW	3B
380	TCH-3	CHAM WALL	C/A THERMOCOUPLE		0-2200 DF	1 CPS	LOW	4A
381	TCH-4	CHAM WALL	C/A THERMOCOUPLE		0-2200 DF	1 CPS	LOW	4B
382	TCH-5	CHAM WALL	C/A THERMOCOUPLE		0-2200 DF	1 CPS	LOW	9B
383	TCH-6	CHAM WALL	C/A THERMOCOUPLE		0-2200 DF	1 CPS	LOW	9C
386	TBP-1	BASE PLATE	I/C THERMOCOUPLE		-100-250 DF	1 CPS	LOW	1B
387	TBP-2	BASE PLATE	I/C THERMOCOUPLE		-100-250 DF	1 CPS	LOW	2A
388	TBP-3	BASE PLATE	I/C THERMOCOUPLE		-100-250 DF	1 CPS	LOW	2C
389	TBP-4	BASE PLATE	I/C THERMOCOUPLE		-100-250 DF	1 CPS	LOW	6C
390	TBP-5	BASE PLATE	I/C THERMOCOUPLE		-100-250 DF	1 CPS	LOW	7C
401	VO-1	OX LINE	6 IN FLOWMETER	200-3600 GPM	200-3600 GPM	1200 CPS	TAPE	
402	VO-2	OX LINE	6 IN FLOWMETER	200-3600 GPM	200-3600 GPM	1200 CPS	TAPE	
403	VF-1	FUEL LINE	12 IN FLOWMETER	900-15K GPM	900-12KGPM	300 CPS	TAPE	

99

INSTRUMENTATION SPECIFICATION SHEET

TEST NUMBER   PROJECT TITLE   DATE

PROJECT 305802305   SHEET 9 OF 1?   SCORPIO-8 ENG CLUSTER, TS1-5A   NOV 196-

ITEM NR.	PARAMETER	LOCATION	TRANSDUCER TYPE	TRANS. RANGE	CAL. RANGE	FREQ. RANGE	REC.SYS.	CHANNEL
404	VF-2	FUEL LINE	12 IN FLOWMETER	900-15K GPM	400-12KGPH	300 CPS	TAPE	
481	F-1	THRUST	LOAD CELL	200 K LBS	0-240 K LBS	200 CPS	OSC	M26
412	F-2	THRUST	LOAD CELL	200 K LBS	0-240 K LBS	1 CPS	L+N	13A
421	ACC-1		ACCELEROMETER		0-350 G	2100 CPS	TAPE	
422	ACC-2		ACCELEROMETER		0-350 G	2100 CPS	TAPE	
423	ACC-3		ACCELEROMETER		0-350 G	2100 CPS	TAPE	
424	ACC-4		ACCELEROMETER		0-350 G	2100 CPS	TAPE	
425	RCC-1		ACCELEROMETER		0-350 G	2100 CPS	TAPE	
426	RCC-2		ACCELEROMETER		0-350 G	2100 CPS	TAPE	
427	RCC-3		ACCELEROMETER		0-350 G	2100 CPS	TAPE	
428	RCC-4		ACCELEROMETER		0-350 G	2100 CPS	TAPE	
429	RCC 1 LEVEL	RCC-1 TP-13				100 CPS	TAPE	
430	RCC 2 LEVEL	RCC-2 TP-13				100 CPS	TAPE	
431	RCC 3 LEVEL	RCC-3 TP-13				100 CPS	TAPE	
432	RCC 4 LEVEL	RCC-4 TP-13					TAPE	
441	SCN-POSITION		CT				TAPE	

INSTRUMENTATION SPECIFICATION SHEET

		TEST NUMBER		PROJECT TITLE			DATE	
				SCORPIO-2 ENG CLUSTER, TSI-5A			NOV 1966	
PROJECT 305902305	SHEET 10 OF 10							
ITEM NR. PARAMETER	LOCATION	TRANSDUCER TYPE	TRANS. RANGE	CAL. RANGE	FREQ.RANGE	REC.SYS.	CHANNEL
442 LCR-POSITION		POT			60.1 CPS	OSC.METER	
443 URS	UP CARRING	SWITCH			135 CPS	OSC	
444 LRS	LOW CARRING	SWITCH			135 CPS	OSC	
445 USS	UP CARRING	SWITCH			135 CPS	OSC	
446 LSS	LOW CARRING	SWITCH			135 CPS	OSC	

REFERENCES

1. Main, H. V., George, D., Franklin, C. E., Mahugh, V. L., Tepe, L. E., Investigation of Large Thrust per Element Injectors with Conventional and Two-Dimensional Thrust Chambers Utilizing Liquid Oxygen and Liquid Hydrogen Propellants, AFRPL-TR-65-149, September 1965. CONFIDENTIAL

2. Main, H. V., George, D., Mahugh, V. L., Tepe, L. E., Oxygen/Hydrogen Injector Thrust per Element Size Maximization, AFRPL-TR-65-199, December 1965. CONFIDENTIAL

3. Plug Cluster Nozzle Study, Pratt & Whitney Aircraft, Contract NAS8-11023, Final Report, PWA FR-1013, September 1964. CONFIDENTIAL

4. Rao, G. V. R., "Approximation of Optimum Thrust Nozzle Contour", ARS Journal Volume 30, Number 6, June 1960.

5. High Pressure Rocket Engine Feasibility Program, Pratt and Whitney Aircraft, AF 04(611)-7435, PWA FR-1171, 10 December 1964. CONFIDENTIAL

6. Goodwin, R., Diller, D., Roder, H., Younglove, B., and Weber, L., Provisional Thermodynamic Functions For Para Hydrogen, NBS Report 6791, 4 August 1961.

7. Liquid Propellant Manual, Unit 8, CPIA, July 1961.

8. Schenck, Hilbert, Jr., Theories of Engineering Experimentation, McGraw-Hill Book Company, Inc., New York, N. Y., 1961.

9. Study for Evaluation of Plug Multichamber Configuration, Pratt and Whitney Aircraft, Contract NAS8-11435, Quarterly Report No. 1, PWA FR-1161, October 1964. CONFIDENTIAL

10. Proposal for Study of Plug Cluster Nozzles for Nova-Type Vehicles, Pratt and Whitney Aircraft, PWA FP 63-64, March 1963.

11. Results of 8-Module Plug Cluster Nozzle Tests, Pratt and Whitney Aircraft, PWA FR-927, February 1964. CONFIDENTIAL

12. Cam Ring Gimbal, Rocketdyne, A Division of North American Aviation, LAPM 62-116.

BIBLIOGRAPHY

1. Sutton, George P., *Rocket Propulsion Elements*, Third Edition, John Wiley and Sons, Inc., New York, N. Y., 1963.

2. *Unique Injector Concepts Development*, Aerojet-General Corporation, Contract AF 04(611)-7410, RTD-TDR-63-1057, September 1963. CONFIDENTIAL

3. *Vortex Combustion*, Reaction Motors Division, Thiokol Chemical Corporation, Contract AF 04(611)-5682, December 1960. CONFIDENTIAL

4. Streeter, Victor L., *Fluid Mechanics*, Second Edition, McGraw-Hill Book Company, Inc., New York, N. Y., 1958.

5. Marks, Lionel S., *Mechanical Engineer's Handbook*, Fifth Edition, McGraw-Hill Book Company, Inc., New York, N. Y., 1951.

6. Shapiro, Ascher H., *Compressible Fluid Flow*, Volume 1, The Ronald Press Company, New York, N. Y., 1953.

7. Main, Howard V., George, D., Mitchell, D., and Smith, K., "Unique Injector Design and Chamber Cooling Techniques", *Bulletin of the Fourth Joint Army-Navy-Air Force-NASA-ARPA Liquid Propulsion Symposium*, Liquid Propellant Information Agency, Silver Spring, Maryland, 8 November 1962. CONFIDENTIAL

DOCUMENT CONTROL DATA - R&D
(Security classification of title, body of abstract and indexing annotation must be entered when the overall report is classified)

1. ORIGINATING ACTIVITY (Corporate author)	2a. REPORT SECURITY CLASSIFICATION
Dept. of the Air Force, AFSC	CONFIDENTIAL
Research and Technology Division	2b. GROUP
AFRPL, Edwards, California 93523	4

3. REPORT TITLE

(U) A Simplified Clustering Technique for Rocket Engine Modules

4. DESCRIPTIVE NOTES *(Type of report and inclusive dates)*

Final Report - Phase III

5. AUTHOR(S) *(Last name, first name, initial)*

George, Daweel   Tepe, Lester E.

Mahugh, 1/Lt Vernon L.   Main, Howard V.

6. REPORT DATE	7a. TOTAL NO. OF PAGES	7b. NO. OF REFS
March 1966	104	12

8a. CONTRACT OR GRANT NO.	9a. ORIGINATOR'S REPORT NUMBER(S)
b. PROJECT NO. 305802405	AFRPL-TR-66-10
c.	9b. OTHER REPORT NO(S) (Any other numbers that may be assigned this report)
d.	

10. AVAILABILITY/LIMITATION NOTICES In addition to security requirements which must be met, this document is subject to special export controls and each transmittal to foreign governments or foreign nationals may be made only with prior approval of AFRPL (RPPR-STINFO), Edwards, California 93523

11. SUPPLEMENTARY NOTES	12. SPONSORING MILITARY ACTIVITY
	See Block 1.

13. ABSTRACT

Results of the tests and evaluations performed on (a) a simplified clustering technique for rocket engine modules, (b) single modules utilizing simplified large thrust per element injectors and film-cooled thrust chambers, and (c) a unique thrust vectoring mechanism known as the Cam Ring Gimbal are presented. This third and final phase of the Scorpio Project was conducted primarily to investigate the cellular combustor concept to attain high thrust. The concept was evaluated in Task B of this phase. In Task A, 44 single-module tests were conducted on two 25,000-pound thrust, simplified injectors with a 45L* film-cooled thrust chamber. The 2 injector configurations were a single-element concentric pentad and a 17-element coaxial pattern, which were selected for testing with the film-cooled chamber as a result of the performance characteristics displayed when they were tested with an uncooled chamber under Phase I of this program. The effect of film cooling on performance, the heat-transfer characteristics, combustion stability, and smooth start and cutoff transients were the major areas of interest. The 17-element coaxial injector was ultimately selected for use in evaluating the cluster concept due to its more uniform heat-flux distribution, thereby according a more efficient utilization of the film-coolant fuel, and its start and stability characteristics. Eight of the simplified, proven modules from Task A were clustered around a common zero-length, altitude-compensating, plug nozzle to demonstrate a simplified clustering technique for discrete assemblies. Only two propellant valves were used for the entire cluster -- one

DD FORM 1473
1 JAN 64

14. KEY WORDS	LINK A		LINK B		LINK C	
	ROLE	WT	ROLE	WT	ROLE	WT
Liquid Rocket Propulsion						
Multi Chamber Configuration						
Simplified Injectors						
Film Cooling						
Thrust Vector Mechanism						
Cryogenic Propellants						
Liquid Oxygen/ Liquid Hydrogen						

13. Abstract (Cont'd):

for the oxidizer, and one for the fuel side. The propellants were transported
to the injectors through manifolds. Thirteen hot firings were conducted on
the cluster configuration. The propellant feed system displayed stable
characteristics, and smooth start and cutoff transients were obtained. All
eight chambers primed within 80 milliseconds. Hot-firing performance
obtained with the plug nozzle correlated very closely with cold-flow data
obtained on a model simulating the Scorpio cluster configuration. Under
Task C of this phase, the Cam Ring Gimbal was incorporated with the cluster
assembly for evaluation under actual hot-firing conditions. The mechanism
consisted of four vertically stacked ring wedges, two of which were movable
to obtain thrust vectoring. The concept was demonstrated feasible in seven
tests, although the gimbal rate achieved was slower than the design rate at
full thrust. The high-energy, cryogenic propellant combination of liquid
oxygen and liquid hydrogen was used throughout the program.